AD-A092 689 STEVENS INST OF TECH HOBOKEN NJ DAVIDSON LAB F/G 13/10
BLADE PRESSURE DISTRIBUTION FOR A MODERATELY LOADED PROPELLER.(U)
SEP 80 S TSAKONAS, J P BRESLIN, W R JACOBS N00014-77-C-0059
UNCLASSIFIED NL

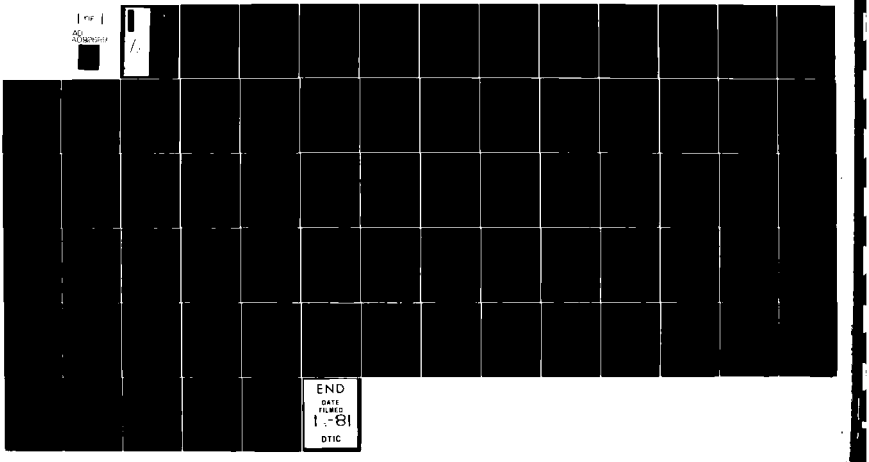

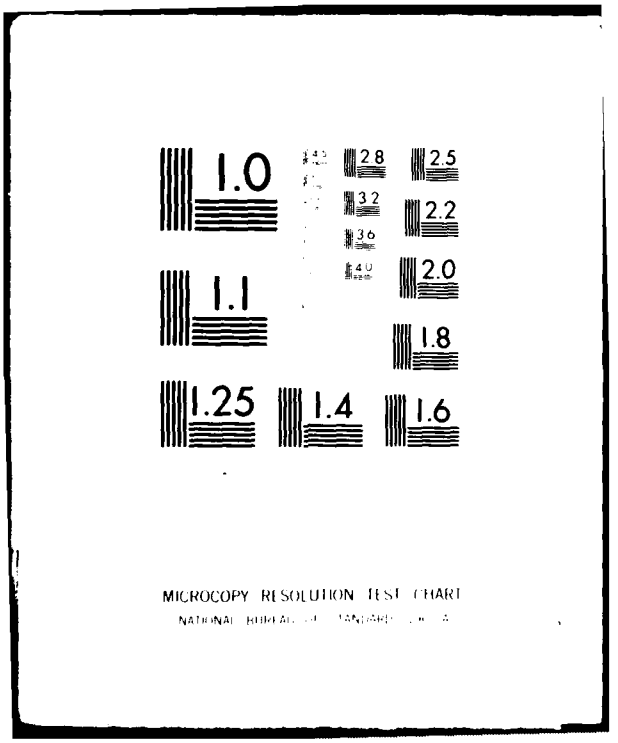
1.0
1.1
1.25
1.4
1.6
1.8
2.0
2.2
2.5
2.8
3.2
3.6
4.0
MICROCOPY RESOLUTION TEST CHART

R-2063

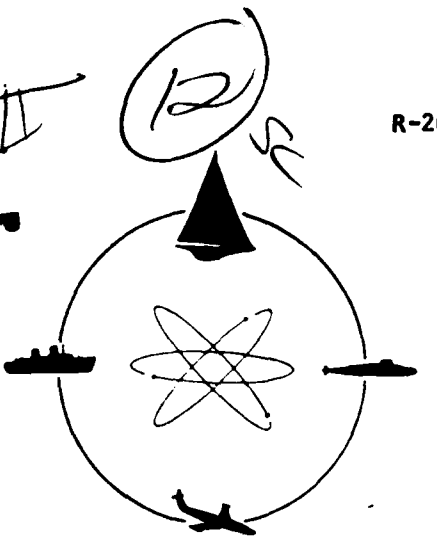

DAVIDSON LABORATORY

Report SIT-DL-80-9-2063
September 1980

BLADE PRESSURE DISTRIBUTION FOR A MODERATELY LOADED PROPELLER

by

S. Tsakonas, J.P. Breslin and W.R. Jacobs

This study was sponsored by the
Naval Sea Systems Command
General Hydromechanics Research Program
Under Contract N000-14-77-C-0059
Administered by
DWT Naval Ship Research and Development Center

(DL Project 4475/009)

STEVENS INSTITUTE
OF TECHNOLOGY

CASTLE POINT STATION
HOBOKEN, NEW JERSEY 07030

UNCLASSIFIED

SECURITY CLASSIFICATION OF THIS PAGE (When Data Entered)

REPORT DOCUMENTATION PAGE	READ INSTRUCTIONS BEFORE COMPLETING FORM
1. REPORT NUMBER: Report SIT-DL-80-9-2063 / 2. GOVT ACCESSION NO.: AD-A092 689	3. RECIPIENT'S CATALOG NUMBER:
4. TITLE (and Subtitle): BLADE PRESSURE DISTRIBUTION FOR A MODERATELY LOADED PROPELLER.	5. TYPE OF REPORT & PERIOD COVERED: FINAL
	6. PERFORMING ORG. REPORT NUMBER:
7. AUTHOR(s): S. Tsakonas, J.P. Breslin and W.R. Jacobs	8. CONTRACT OR GRANT NUMBER(s): N000414-77-C-0059
9. PERFORMING ORGANIZATION NAME AND ADDRESS: Davidson Laboratory / Stevens Institute of Technology / Castle Point Station, Hoboken, NJ 07030	10. PROGRAM ELEMENT, PROJECT, TASK AREA & WORK UNIT NUMBERS: 61153N RO2301 / SR 023 01 01
11. CONTROLLING OFFICE NAME AND ADDRESS: David W. Taylor Naval Ship Research and Development Center, Code 1505 / Bethesda, MD 20084	12. REPORT DATE: September 1980
	13. NUMBER OF PAGES: x + 59 pp.
14. MONITORING AGENCY NAME & ADDRESS (if different from Controlling Office): Office of Naval Research / 800 N. Quincy Street / Arlington, VA 22217	15. SECURITY CLASS. (of this report): UNCLASSIFIED
	15a. DECLASSIFICATION/DOWNGRADING SCHEDULE:

16. DISTRIBUTION STATEMENT (of this Report)

APPROVED FOR PUBLIC RELEASE; DISTRIBUTION UNLIMITED

17. DISTRIBUTION STATEMENT (of the abstract entered in Block 20, if different from Report)

18. SUPPLEMENTARY NOTES

Sponsored by the Naval Sea Systems Command General Hydromechanics Research Program administered by the David W. Taylor Naval Ship Research and Development Center, Code 1505, Bethesda, MD 20084.

19. KEY WORDS (Continue on reverse side if necessary and identify by block number)

Hydrodynamics
Moderately Loaded Propellers
Blade Pressure Distribution

20. ABSTRACT (Continue on reverse side if necessary and identify by block number)

A new theoretical procedure has been developed modifying the existing analysis for a marine propeller operating in a nonuniform inflow field by considering the radially varying mean wake and mean propeller induction. In addition, the selection of a new reference surface around which the perturbation analysis is developed is based on the nonlinear form of the Bernoulli equation together with an appropriate kinematic condition

(Continued)

DD FORM 1 JAN 73 1473 EDITION OF 1 NOV 65 IS OBSOLETE
S/N 0102-014-6601

UNCLASSIFIED
SECURITY CLASSIFICATION OF THIS PAGE (When Data Entered)

20. Abstract (Cont'd)

existing at the propeller operational condition. A flow field closer to the propeller operating condition is achieved thereby and the linear theory requirement of small perturbation quantities is reinforced. The approach is thus applicable to moderately to heavily loaded propellers immersed in the stronger wakes of hulls of large block coefficient, although it can be used for lightly loaded propellers as well.

STEVENS INSTITUTE OF TECHNOLOGY
DAVIDSON LABORATORY
CASTLE POINT STATION
HOBOKEN, NEW JERSEY

Report SIT-DL-80-9-2063

September 1980

BLADE PRESSURE DISTRIBUTION FOR A MODERATELY LOADED PROPELLER

by

S. Tsakonas, J.P. Breslin and W.R. Jacobs

This study was sponsored by the

Naval Sea Systems Command
General Hydromechanics Research Program
Under Contract N000-14-77-C-0059
Administered by
DWT Naval Ship Research and Development Center
(DL Project 4475/009)

A

Approved:

John P. Breslin

John P. Breslin
Director

x + 59 pp.

APPROVED FOR PUBLIC RELEASE; DISTRIBUTION UNLIMITED

ABSTRACT

A new theoretical procedure has been developed modifying the existing analysis for a marine propeller operating in a nonuniform inflow field by considering the radially varying mean wake and mean propeller induction. In addition, the selection of a new reference surface around which the perturbation analysis is developed is based on the nonlinear form of the Bernoulli equation together with an appropriate kinematic condition existing at the propeller operational condition. A flow field closer to the propeller operating condition is achieved thereby and the linear theory requirement of small perturbation quantities is reinforced. The approach is thus applicable to moderately to heavily loaded propellers immersed in the stronger wakes of hulls of large block coefficient, although it can be used for lightly loaded propellers as well.

KEYWORDS

Hydrodynamics
Moderately Loaded Propellers
Blade Pressure Distribution

TABLE OF CONTENTS

NOMENCLATURE

$A(x)$	function defined in Eq.(17)
$a(r)$	inverse advance ratio (Eq.4)
a_e	effective inverse advance ratio (Eq.41)
$\bar{a}$	designation of NACA-a meanline
C_P	pressure coefficient
$C(r)$	expanded chord length, ft
$F_{x,y,z}$	propeller-induced forces in x,y,z direction
f_c	camberline ordinates from face pitch line
f_T	blade thickness distribution over one side of blade section
$I_m(\ )$	modified Bessel function of first kind, of order m
$I^{(\bar{m})}(\ )$	defined in Eq.(6)
i	index
J_d	design advance ratio
J_{od}	off-design advance ratio
ΔJ	$J_{od}-J_d$
j	index
K	kernel of integral equation
$\bar{K}^{(\bar{m},\bar{n})}$	modified kernel after chordwise integrations
$K_m(\ )$	modified Bessel function of second kind of order m
k	variable of integration
$L^{(q)}(\rho,\theta_\alpha)$	loading distribution in lb/ft
$L^{(q)}(r)$	spanwise loading in lb/ft
$L^{(q,\bar{n})}(\rho)$	spanwise loading coefficients of the chordwise modes in lb/ft
ℓ	integer multiple
M_b	blade bending moment about face pitch line

$M(\xi,\rho,\theta_o)$	source strength at point (ξ,ρ,θ_o)
m	index of summation
$\bar{m}$	order of lift operator
N	number of blades
n	blade index
n	rps
$\bar{n}$	order of chordwise mode
$\vec{n}$	unit normal vector on helicoidal surface at loading point
$\vec{n}'$	unit normal vector on helicoidal surface at control point
P,p	pressure, lb/ft^2
ΔP	$P_- - P_+$, pressure jump, lb/ft^2
P(r)	geometric pitch at each radial position, ft
$Q_{x,y,z}$	propeller-induced moments about x,y,z axis
q	order of harmonic of inflow field
R	Descartes distance
r	radial ordinate of control point
r_o	propeller radius, ft
S	propeller lifting surface, ft^2
s	chordwise location as fraction of chord length
t	time, sec
t_o	maximum thickness of blade, ft
U	free stream velocity, ft/sec (design)
$U_A(r)$	local speed of advance, ft/sec (design)
$U_A(r)_{od}$	local speed of advance, ft/sec (off design)
u	variable of integration
u_i,v_i,w_i	axial, tangential and radial components of perturbation velocities
$V^{(q)}(r)$	Fourier coefficients of the known downwash velocity distribution

V_c	normal velocity due to camber effects
V_f	normal velocity due to flow-incidence angle
V_N	normal velocity due to wake
V_τ	normal velocity due to nonplanar thickness
V_L	longitudinal perturbation velocity (V_x-U_A)
V_T	tangential perturbation velocity
V_x	measured axial velocity
W_r	mean wake velocity in radial direction
x	longitudinal ordinate of control point
x,r,φ	cylindrical coordinates of control point
x,y,z	Cartesian coordinate system
$\beta(r)$	$\tan^{-1}(1/a(r)r)$
δ	defined in Eq.(4)
$\Theta(\vec{n})$	chordwise mode shapes
Θ	$-\Omega t$
θ	angular ordinate of loading point
θ_o	angular position of loading point with respect to blade reference line, in moving coordinate system
θ_b	subtended angle of projected blade semichord, radians
$\bar{\theta}_n$	$2\pi(n-1)/N$, n=1,2, ... N
$\theta_p(r)$	geometric pitch angle at each radial position
θ_α	angular chordwise location of loading point
$\Lambda^{(\vec{n})}(y)$	defined in Eq.(6) (see Appendix A)
$\Lambda_1^{(\vec{n})}(y)$	defined in Appendix A
ξ	longitudinal ordinate of loading point
ξ,ρ,θ	cylindrical coordinates of loading point
ρ	radial ordinate of loading point
ρ_f	mass density of fluid

ρ_o	ratio of leading edge radius to chord
σ	angular measure of skewness from blade reference line
$\Delta\sigma$	$\sigma^r - \sigma^\rho$ = difference in skewness at control and loading point
τ	variable of integration
Φ	velocity potential
$\Phi(\bar{m})$	generalized lift operator
φ	angular ordinate of control point
φ_o	angular position of control point with respect to blade reference line, in moving coordinate system
φ_α	angular chordwise location of control point
Ψ	acceleration potential
Ω	magnitude of angular velocity of propeller

Superscripts

r	refers to control point
ρ	refers to loading point

INTRODUCTION

In the course of a series of investigations concerned with adaptation of the unsteady lifting surface theory to marine propellers,[1,2*] the following basic assumptions have been made:

a) the propeller operates in a spatially nonuniform, nonseparating and noncavitating flow of an inviscid and incompressible fluid,

b) all perturbation quantities are considered to be small, so that the linearized version of the theory may be used as a basis,

c) a helicoidal surface of constant pitch (from hub-to-tip) is selected as reference surface and deviations from this surface are considered as the perturbation quantities.

The reference surface, over which the singularities are distributed, is the "zero lift" helicoidal with constant pitch $2\pi \frac{U}{\Omega}$ where U is the forward speed (ship speed) and Ω the angular velocity of the rotating propeller. Any deviation from this surface is taken to be induced by perturbation velocities such as those due to ship wake, incident flow angle, blade camber, non-planar blade thickness and flow-distortion blade thickness. These effects have been considered separately and then, as permitted in the linear theory, have been added together to determine their combined effects on the loading and hydrodynamic forces. The linearized version of the unsteady lifting surface theory leads to an integral equation relating the unknown loading distribution with the known onset velocities. The equation is valid for a lightly loaded propeller with wakes of small magnitude (intensity). With today's tendency toward longer and fuller hull forms, the wake intensity behind the hull is quite strong. Thus the perturbation quantities are larger so that the linearized theory is inadequate for the needs of the propeller designer in regard to the prediction of mean thrust and torque.

*Superior numbers in text matter refer to similarly numbered references listed at the end of this report.

The propeller operating in ship wake which varies with radial and angular position not only encounters the spatial inhomogeneities of the incoming flow but it is also under the influence of the self-induced velocity field. The latter can be determined provided the blade loadings are known which, in effect, requires "apriori" knowledge of the reference surface. Thus an iterative procedure must be established based, as a first step, on an assumed helicoidal reference surface determined by the known variable hydrodynamic pitch angle from which the first approximations of blade loading and propeller induction are determined. Having this induction and the radial variation of the speed of advance a new reference surface is established and thus another set of calculations is performed for the evaluation of the new blade loading and induction effect. The iterative procedure is continued until no variation in the pitch of the reference surface and in the blade loading can be observed.

While the iterative procedure uses the same linearized approach as developed in Reference 1, it takes into account the quadratic form of the Bernoulli equation, since the pertubation velocities are sometimes of the same order of magnitude as the velocities of the undisturbed flow in which case linearization of the pressure equation is not valid. This procedure is appropriate to moderately loaded propeller operational conditions. Once the final geometry of the reference surface is established, the solution of the integral equation relating the unknown loading with the known onset velocities will determine the blade pressure distribution and the corresponding hydrodynamic forces. It should be noted that the imposed boundary conditions on the blade are fixed and do not change during the iterative process.

The same reference surface is further used for the unsteady flow conditions, since the unsteady onset velocities being small compared to steady state velocities can be considered as perturbation without running the risk of violating the basic requirements of the linearized theory.

This study is sponsored by the Naval Sea Systems Command General Hydrodynamics Research Program under Contract N00014-77-C-0059, administered by the David Taylor Naval Ship Research and Development Center.

ANALYSIS

1) Integral Equation

A theory and computer program have been developed for the case of a lightly loaded propeller utilizing the small perturbation approximation by selecting as a reference surface the helicoidal surface of "zero lift" with constant pitch (i.e., $P = 2\pi \frac{U}{\Omega} = \frac{2\pi}{a}$ where U = ship speed and Ω = propeller rotational velocity). However, many propellers operate in strong wakes and at lower relative inflow velocities resulting in larger deviation from the reference surface hitherto employed. These large excursions violate the requirement of the small perturbation theory.

A new analysis is developed herein along the same general lines as the small perturbation theory but with emphasis on the selection of a more appropriate reference surface which simulates closely the actual propeller operational conditions.

The linearized unsteady lifting surface theory for a marine propeller, with its blades lying on a helicoidal surface and operating in the nonuniform flow of an incompressible ideal fluid, is formulated by means of acceleration potential method. It is based not only on a small perturbation approximation but, also, on the assumptions that the propeller blades are thin and operate without cavitation and flow separation.

It may now be considered, more appropriately, that this propeller operates in a spatially varying flow generated by a strong hull wake and also under the influence of self-induction. Both these factors will influence the selection of the proper reference surface in the steady state flow conditions. It is assumed that the flow field in which the propeller is immersed has velocity components given in cylindrical coordinates by

$$U_A(r) + u_i(x,r);\ v_i(x,r);\ w_i(x,r) \qquad (1)$$

where $U_A(r)$ is the local speed of advance and u_i, v_i, w_i are the axial, tangential and radial components of the perturbation velocities.

The relation between the velocity potential function Φ and the acceleration potential function ψ has been established by solving the linearized Euler equation of motion to obtain

$$\Phi(x,r,\varphi;t) = \frac{1}{U(r)} \int_{-\infty}^{x} \psi(\tau,r,\varphi;t - \frac{x-\tau}{U(r)})\, d\tau \qquad (2)$$

where $U(r) = U(o,r) = U_A(r) + u_i(o,r)$ the axial component of the resulting velocity at the propeller plane.

It is further known that the pressure field generated by a lifting surface S is given by distributed doublets with axis parallel to the local normal and with strength equal to the pressure jump across the surface. The reference surface over which the doublets are distributed is a helicoidal surface with variable pitch along the radius. These facts considered with Equation (2) lead (following Reference 1) to an integral equation which relates the known onset velocities with the unknown blade loading at each frequency q:

$$V(r)e^{-iq\varphi_o} = \iint_S \Delta p^{(q)}(\xi,\rho,\theta_o)\, K(r,\varphi_o;\rho,\theta_o;q)\, dS \qquad (3)$$

where the kernel function is given by

$$K(r,\varphi_o;\rho,\theta_o;q) = -\frac{1}{4\pi\rho_f U(r)} \lim_{\delta\to o} \sum_{n=1}^{N} e^{-iq\bar{\theta}_n} \frac{\partial}{\partial n'} \int_{-\infty}^{x} e^{iqa(r)(\tau-x)} \frac{\partial}{\partial n}\left(\frac{1}{R}\right) d\tau \qquad (4)$$

Here

$$a(r) = \frac{\Omega r + v_i(r)}{U_A(r) + u_i(r)}$$

Ω = angular propeller velocity

$U_A(r)$ = speed of advance at the propeller plane at radial location r

$\delta \to o$ means $x \to \varphi_o/a(r)$ and $\xi \to \theta_o/a(\rho)$

$\bar{\theta}_n = 2\pi(n-1)/N \quad n = 1,2 \ldots N$

N = number of blades

R = Descartes distance between the control point (x,r,φ_o) and loading point $(\xi,\rho,\theta_o) = \left[(\tau-\xi)^2+r^2+\rho^2-2r\rho\cos(\theta_o-\varphi_o+\theta_n-a(r)(\tau-x)\right]^{\frac{1}{2}}$

$$\frac{\partial}{\partial n} = \frac{\rho}{\sqrt{1 + a^2(\rho)\rho^2}} \left(a(\rho) \frac{\partial}{\partial \xi} - \frac{1}{\rho^2} \frac{\partial}{\partial \theta_o}\right)$$

and

$$\frac{\partial}{\partial n'} = \frac{r}{\sqrt{1 + a^2(r)r^2}} \left(a(r) \frac{\partial}{\partial x} - \frac{1}{r^2} \frac{\partial}{\partial \varphi_o}\right)$$

are the normal derivatives at the loading and control point, respectively. It should be noted that the time factor has been eliminated from both sides of Eq. (3) and it is understood that only the real part of the solution is retained. A limiting process is introduced in the kernel function to avoid the mathematical difficulty due to the presence of a high order singularity. The kernel function being one of the most complex in the lifting surface theory, attention is given to the numerical solution of the integral equation by means of a high-speed digital computer. The analysis, however, has been carried out to the stage where laborious computations can be efficiently performed by the numerical procedure.

It has been assumed that the shape of the chordwise loading is the same as has been shown by Landahl to be the appropriate one in a two-dimensional flow. Furthermore, a method called the "generalized lift operator" technique[3] is applied to both sides of the integral equation to reduce the surface integral equation to a line integral equation along the propeller radius. Then by the collocation method

the line integral equation is reduced to a set of algebraic equations in the unknown spanwise loading distribution.

The following substitutions are made in Equations 3 and 4:

$$L^{(q)}(\rho,\theta_\alpha) = \Delta p^{(q)}(\xi,\rho,\theta_o) \cdot \rho\theta_b^\rho \quad \text{lb/ft}$$

$$\theta_o = \sigma^\rho - \theta_b^\rho \cos\theta_\alpha \qquad 0 \le \theta_\alpha \le \pi$$

$$\varphi_o = \sigma^r - \theta_b^r \cos\varphi_\alpha \qquad 0 \le \varphi_\alpha \le \pi$$

and the expansion of the inverse Descartes distance is

$$\frac{1}{R} = \frac{1}{\pi} \sum_{m=-\infty}^{\infty} e^{im[\theta_o-\varphi_o+\bar{\theta}_n-a(r)(\tau-x)]} \int_{-\infty}^{\infty} I_m(|k|\rho)K_m(|k|r)e^{i(\tau-\xi)k}\,dk$$

for $\rho < r$ (otherwise ρ and r in the modified Bessel functions must be interchanged). Here σ is the propeller skewness (the angular position of the midchord line from the generator line through the hub in the projected propeller plane), θ_b is the subtended angle of the projected blade semichord, θ_α and φ_α are angular chordwise locations of the loading and control points, respectively, and the superscripts ρ and r refer to the values at the loading and control points, respectively.

After the chordwise integration and application of the lift-operator, the integral Eq. (3) reduces to:

$$\frac{V^{(q)}(r)}{U_A(r)} e^{-iq\sigma^r} I^{(\bar{m})}(q\theta_b^r) = \sum_{\bar{n}=1}^{\bar{n}max} \int_\rho L^{(q,\bar{n})}(\rho)\bar{K}^{(\bar{m},\bar{n})}(r,\rho;q)d\rho \quad (5)$$

and

$$\bar{K}(\bar{m},\bar{n}) = -\frac{N}{4\pi\rho_f U_A(r)U(r)}\,\frac{r}{a(\rho)\left[1+a^2(r)r^2\right]}\sum_{\substack{m=-\infty\\ m=q+\ell N}}^{\infty} e^{-iq\Delta\sigma}$$

$$\cdot\left\{e^{i\ell N\left(1-\frac{a(r)}{a(\rho)}\right)\sigma^{\rho}}\left[a^2(r)\ell N+\frac{m}{r^2}\right]\left[a(\rho)a(r)\ell N+\frac{m}{\rho^2}\right]I^{(\bar{m})}(q\theta_b^r)\Lambda^{(\bar{n})}\left[\left(q+\left(1-\frac{a(r)}{a(\rho)}\right)\ell N\right)\theta_b^{\rho}\right]\right.$$

$$\cdot\, I_m(a(r)|\ell N|\rho)\, K_m(a(r)|\ell N|r)$$

$$-\frac{i}{\pi}e^{-i\ell N\Delta\sigma}\int_{-\infty}^{\infty}\left(a(r)k+\frac{m}{r^2}\right)\left(a(\rho)k+\frac{m}{\rho^2}\right)e^{ik\left(\frac{\sigma^r}{a(r)}-\frac{\sigma^{\rho}}{a(\rho)}\right)}\frac{I_m(|k|\rho)K_m(|k|r)}{k-a(r)\ell N}$$

$$\left.\cdot\, I^{\bar{m}}\left(\left(m-\frac{k}{a(r)}\right)\theta_b^r\right)\Lambda^{\bar{n}}\left(\left(m-\frac{k}{a(\rho)}\right)\theta_b^{\rho}\right)\,dk\right\}. \qquad (6)$$

and $\Delta\sigma = \sigma^r - \sigma^{\rho}$.

Here

$$I^{\bar{m}}(y) = \frac{1}{\pi}\int_0^{\pi}\Phi(\bar{m})\, e^{iy\cos\varphi_\alpha}\, d\varphi_\alpha$$

and

$$\Lambda^{\bar{n}}(z) = \frac{1}{\pi}\int_0^{\pi}\Theta(\bar{n})\, e^{-iz\cos\theta_\alpha}\sin\theta_\alpha\, d\theta_\alpha$$

the details of which are presented in Appendix A.

The integral equation (5) is solved numerically by the usual collocation method with the loading $L^{(q,\bar{n})}(\rho)$ assumed to be constant over each small radial strip. Then only the kernel needs to be integrated over the radial strip.

Reference 1 gives details of the analytical development and the different numerical procedures used to obtain the finite contributions of the Cauchy-type singularity of the k-integral at $k = a(r) \cdot (m - q)$ and of the higher-order Hadamard-type singularity when $\rho = r$.

2) Chordwise Modes

The proper selection of chordwise modes is dictated by the loading distribution on a foil in two-dimensional flow conditions. The same chordwise modes have been selected as those of Reference 2 .

a) Unsteady flow conditions

The unknown chordwise modes are approximated by the known Birnbaum distribution which has the proper leading edge singularity and satisfies the Kutta condition at the trailing edge.

$$L^{(q)}(\rho,\theta_\alpha) = \sum_{\bar{n}=1}^{\bar{n}max} L^{(q,\bar{n})}(\rho)\,\Theta(\bar{n})$$

$$= \frac{1}{\pi}\left\{L^{(q,1)}(\rho)\cot\frac{\theta_\alpha}{2} + \sum_{\bar{n}=2}^{\bar{n}max} L^{(q,\bar{n})}(\rho)\sin(\bar{n}-1)\theta_\alpha\right\} \tag{7}$$

b) Steady state flow conditions

The unknown chordwise mode shapes are selected to conform to the observed pressure distribution on the NACA foil sections.

i) The NACA-$\bar{a}$ mean line at the design condition

The section has a constant loading distribution from $\frac{x}{c} = o$ at the leading edge to $\frac{x}{c} = \bar{a}$ ($\bar{a}$ varying from 0 to 1; x = location of points along the chord and c = chord length) and then decreases linearly to zero at $\frac{x}{c} = 1$, the trailing edge. This type is designated as "roof-top" loading and the distribution is given by

$$L^{(o)}(\rho,\theta_\alpha) = L^{(0,1)}(\rho)\Theta(1) = \begin{cases} L(\rho)^{(0,1)} & 0 \le x \le \bar{a} \\ L(\rho)^{(0,1)}\,\dfrac{1-x}{1-\bar{a}} & \bar{a} \le x \le 1 \end{cases} \tag{8}$$

with the corresponding $\Lambda^{(1)}(z)$ given in Appendix A.

ii) For any other sections such as NACA mean lines of the 4- and 5-digit wing series, including the lenticular mean line, and arbitrary mean lines in general the distribution is

$$L^{(o)}(\rho,\theta_\alpha) = \frac{1}{\pi} \sum_{\bar{n}=1}^{\bar{n}max} L^{(o,\bar{n})}(\rho)\, \Theta(\bar{n})$$

$$= \frac{1}{\pi}\left\{L^{(o,1)}(\rho)\cot\frac{\theta\alpha}{2} + \sum_{\bar{n}=2}^{\bar{n}max} L^{(o,\bar{n})}(\rho)\sin(\bar{n}-1)\theta_\alpha\right\} \quad (9)$$

iii) Off-design flow condition

If the solution of the integral equation at the design flow condition is known, (J_d = advance ratio at the design condition) then the off-design condition can be obtained through the input arrangement. In the steady state flow conditions at off-design advance ratio J_{od}, the propeller is subjected to a change in angle of attack due to $\Delta J = J_{od} - J_d$. The additional loading due to this additional change of angle of attack will be obtained by utilizing as chordwise loading distribution the first term of the Birnbaum distribution, i.e.,

$$L^{(o)}(\rho,\theta_\alpha) = \frac{1}{\pi} L^{(o)}(\rho)\cot\frac{\theta_\alpha}{2} \quad (10)$$

If, however, the information on the design flow condition is not available then the general form of the Birnbaum distribution should be used for the chordwise loading distribution

$$L^{(o)}(\rho,\theta_\alpha) = \frac{1}{\pi}\left\{L^{(0,1)}(\rho)\cot\frac{\theta_\alpha}{2} + \sum_{\bar{n}=1}^{\infty} L^{(o,\bar{n})}(\rho)\sin(\bar{n}-1)\theta_\alpha\right\}$$

(11)

3) Perturbation Velocity Distributions

The left-hand side of the integral equation represents the normal component of the velocity perturbations from the basic flow due to non-uniformity of the flow (wake), to blade camber, non-planar blade thickness and the incident flow angle in the design conditions, and to an additional flow angle in the off-design condition arising from the difference between off-design and design advance ratios.

a) Normal velocity due to wake

The normal component of the wake velocity along the middle chord of each radial strip is given by (cf Reference 2)

For q = 0

$$\frac{V_N(r)}{U_A(r)} = \frac{V_L(r)}{U_A(r)} \cos\theta_p(r) - \frac{V_T(r)}{U_A(r)} \sin\theta_p(r)$$

where

$$\frac{V_L(r)}{U_A(r)} \approx \frac{V_X(r)}{U_A(r)} \quad \ldots 1$$

$\frac{V_X(r)}{U_A(r)}$ = measured axial velocity normalized with respect to the speed of advance

$\frac{V_T(r)}{U_A(r)}$ = measured tangential velocity normalized with respect to the speed of advance

θ_p = blade pitch angle = $\tan^{-1} \frac{P(r)}{2\pi r}$

For a single screw ship $V_T^{(o)} = 0$ and taking $V_X^{(r)} = U_A(r)$ then

$$\frac{V_N^{(o)}(r)}{U_A(r)} = 0$$

Thus there is no wake distribution in the steady state case when the reference surface is selected on the basis of the velocity of advance.

For $q \neq 0$

The input to the program is

$$\left(\frac{V_N^{(q)}}{U_A^{(r)}}\right)_R = a_q(r)\cos\theta_p(r) - A_q(r)\sin\theta_p(r)$$

$$\left(\frac{V_N^{(q)}}{U_A^{(r)}}\right)_I = b_q(r)\cos\theta_p(r) - B_q(r)\sin\theta_p(r) \qquad (12)$$

where R and I represent the real and imaginary parts. The coefficients a, b, A and B are obtained from the harmonic analysis of the wake survey:

$$\frac{V_X(r)}{U_A^{(r)}} = \sum_{q=1}^{\infty}\left[a_q(r)\cos q\Theta + b_q(r)\sin q\Theta\right]$$

$$\frac{V_T^{(r)}}{U_A^{(r)}} = \sum_{q=1}^{\infty}\left[A_q(r)\cos q\Theta + B_q(r)\sin q\Theta\right]$$

The same sign convention as in Reference 2 has been utilized. The positive Θ is defined in the counterclockwise direction from $\Theta = 0$ at the upright position of the blade. The axial component V_x is positive downstream and tangential component V_T is positive in the counterclockwise direction looking upstream.

b) Normal velocity due to blade camber

The velocity V_c normal to the blade in the negative direction induced by the flow disturbance caused by blade camber is given by

$$\frac{V_C^{(o)}(r)}{U_A(r)} = \frac{\sqrt{1+a_A^2(r)r^2}}{C(r)}\frac{\partial f_C(r,s)}{\partial s}$$

$$= \frac{2\sqrt{1+a_A^2(r)r^2}}{C(r)\sin\varphi_\alpha}\frac{\partial f_C(r,\varphi_\alpha)}{\partial \varphi_\alpha} \qquad (13)$$

where

$\frac{\partial f_C(r,s)}{\partial s}$ = slope of the camber line $f_C(r,s)$ measured from the face pitch line

$s = \frac{1}{2}(1-\cos\varphi_\alpha)$ chordwise location non-dimensionalized on the basis of $C(r)$

$C(r)$ = chord in feet

$a_A(r)$ = $\Omega r/U_A(r)$

On applying the lift-operator to the above expression, then

$$\frac{\bar{V}_C^{(o)}(r)}{U_A(r)} = \frac{2\sqrt{1+a_A^2(r)r^2}}{\pi C(r)} \int_o^\pi \Phi(\bar{m}) \frac{\partial f_C}{\partial \varphi_\alpha} \frac{d\varphi_\alpha}{\sin\varphi_\alpha} \qquad (14)$$

where $\Phi(\bar{m})$ = lift operator defined in Appendix A.

The integration is done as in Reference 4. In the small range near the leading edge $0 \le \varphi_\alpha \le \cos^{-1}(0.9)$ or $0 \le s \le 0.05$ the camberline is assumed to be parabolic and in the range $\cos^{-1}(-.8) \le \varphi_\alpha \le \pi$ or $0.90 \le s \le 1.0$ near the trailing edge, the camberline is assumed to be straight line. The integration is done analytically in these regions and numerically over the remainder of the chord.

c) Normal velocity due to "non-planar" blade thickness

The thickness of propeller blades describing a helicoidal surface or non-planar surface generates a velocity field on the blade itself and consequently, affects the loading distribution in the steady state.

Resorting to the "thin body" approximation, the velocity potential Φ_T due to the blade thickness of an N-blade propeller is given by

$$\Phi_T(x,r,\varphi_o) = -\frac{1}{4\pi} \sum_{n=1}^{N} \int_{\theta_o} \int_{\rho} \frac{M(\xi,\rho,\theta_o)}{R} \frac{\sqrt{1+a_A^2(\rho)\rho^2}}{a_A(\rho)\rho} \, \rho d\rho d\theta_o \qquad (15)$$

where

$$M(\xi,\rho,\theta_o) = 2U_A(\rho)\sqrt{1+a_A^2(\rho)\rho^2}\,\frac{\partial f_\tau(\rho,s)}{\partial s}$$
$$= 2U_A(\rho)\,\frac{\partial f_\tau(\xi,\rho,\theta_o)}{\partial \xi}$$

$f_\tau(\xi,\rho,\theta_o)$ = thickness distribution over <u>one side</u> of the blade section at radial position ρ in the propeller plane.

$$R = [(x-\xi)^2 + r^2 + \rho^2 - 2r\rho\cos(\theta_o-\varphi_o+\bar{\theta}_n)]^{\frac{1}{2}}$$

$$\bar{\theta}_n = \frac{2\pi(n-1)}{N}\,, \quad n = 1,2 \ldots N$$

θ_o,φ_o = angular position of the loading and control points, respectively, from the reference line (see Figure 1)

The corresponding normal velocity component is given by

$$\frac{V_\tau^{(o)}(r)}{U_A(r)} = -\frac{1}{U_A(r)}\,\frac{\partial \Phi_\tau(x,r,\varphi_o)}{\partial n'} \qquad (16)$$

The application of the lift operator after the use of the transformations

$$x = \frac{\varphi_o}{a_A(r)} = (\sigma^r - \theta_b^r\cos\varphi_\alpha)/a_A(r) \qquad 0 \le \varphi_\alpha \le \pi$$

$$\xi = \frac{\theta_o}{a_A(\rho)} = (\sigma^\rho - \theta_b^\rho\cos\theta_\alpha)/a_A(\rho) \qquad 0 \le \theta_\alpha \le \pi$$

and the expansion of $1/R$ in a series yields (see Appendix B)

$$\frac{V_\tau^{(o)}(r)}{U_A(r)} = -\frac{Nr}{\pi^2 U_A(r)\sqrt{1+a_A^2(r)r^2}}\int_\rho U_A(\rho)\sqrt{1+a^2(\rho)\rho^2}$$

$$\cdot\left\{\int_o^\infty a_A(r)u I_o(u\rho)K_o(ur)\left[\text{Im.Part}\left\{1^{(\bar{m})}\left(-u\theta_b^r/a_A(r)\right)A\left(u\theta_b^\rho/a_A(\rho)\right)e^{iu(\sigma^r/a_A(r)-\sigma^\rho/a_A(\rho))}\right\}\right]du\right.$$

$$\left. + \sum_{\ell=1}^{\infty}\int_o^\infty I_{\ell N}(u\rho)K_{\ell N}(ur)\,[G(u,\ell) + G(u,-\ell)]du\right. \qquad (17)$$

where

$$G(u,\ell)=\left[a_A(r)u+\frac{\ell N}{r^2}\right]\text{Im.Part}\left[I^{(\bar{m})}\left(\left(a_A(r)\,\ell N-u\right)\theta_b^r/a_A(r)\right)A\left(\left(u-a_A(\rho)\,\ell N\right)\theta_b^\rho/a_A(\rho)\right)\right.$$

$$\left.\cdot\, e^{-i\ell N(\sigma^r-\sigma^\rho)}\, e^{iu(\sigma^r/a_A(r)-\sigma^\rho/a_A(\rho))}\right]$$

and

$$A(x)=\int_0^\pi \frac{\partial f_\tau}{\partial\theta_\alpha}\, e^{ix\cos\theta_\alpha}\, d\theta_\alpha$$

which can be evaluated once the thickness distribution $f(\tau)$ is supplied.

For any propeller the blade semi-thickness distribution in the projected plane can be approximated by (see Reference 2)

$$f_\tau(\rho,\theta_\alpha)\simeq 2\rho\theta_b^\rho\left\{\sqrt{2\rho_o(\rho)}\,\sin\frac{\theta_\alpha}{2}+\frac{t_o(\rho)}{C(\rho)}\left[a_o(\rho)+\sum_{n=1}^{4}a_n(\rho)\cos n\theta_\alpha\right]\right\} \quad (18)$$

where f_τ and ρ are fractions of propeller radius r_o

$\rho_o(\rho)$ = ratio of leading edge radius to chord length $C(\rho)$ at given radial position

t_o/C = ratio of maximum thickness to chord at that radial position

The coefficients $a_o(\rho)$ and $a_n(\rho)$ are determined from the equivalent fourth order polynomial in x by the "least squares" method as shown in Reference 2 .

d) Normal velocity due to flow angle.

The incident flow angle has been defined as the difference between the geometric pitch angle $\theta_p(r)=\tan^{-1}\frac{P(r)}{2\pi r}$ and the hydrodynamic pitch angle $\beta(r)=\tan^{-1}\left(\frac{1}{a(r)r}\right)$ of the reference helicoidal surface. The normal velocity due to this effect is then given by

$$\frac{V_f^{(o)}(r)}{U_A(r)} = -\sqrt{1 + a_A^2(r)r^2}\left(\theta_p(r) - \tan^{-1}\frac{1}{a_A(r)r}\right)$$

which after the application of the lift operator becomes

$$\frac{\bar{V}_f^{(o,\bar{m})}}{U_A(r)} = \begin{cases} -\sqrt{1 + a_A^2(r)r^2}\left(\theta_p - \tan^{-1}\frac{1}{a_A(r)r}\right) & \text{for } \bar{m} = 1 \text{ or } 2 \\ 0 & \text{for } \bar{m} > 2 \end{cases} \tag{19}$$

since $l^{(1)}(0) = l^{(2)}(0) = 1$ and $l^{(\bar{m})}(0) = 0$ for $\bar{m} > 2$.

At off-design advance ratio J_{od}, the propeller is subjected to a change in angle of attack due to $\Delta J = J_{od} - J_d$. The normal velocity perturbation due to this change in angle of attack is given by

$$\frac{\Delta\bar{V}_f^{(o,\bar{m})}}{U_{od}(r)} = \left\{ -\sqrt{1 + a_{od}^2(r)r^2}\left[\theta_p(r) - \tan^{-1}\frac{1}{a_{od}(r)r}\right] + \sqrt{1 + a_d^2(r)r^2}\left[\theta_p(r) - \tan^{-1}\frac{1}{a_d(r)r}\right]\frac{U_d(r)}{U_{od}(r)}\right\} \tag{20}$$

for $\bar{m} = 1$ and 2.

$U_{od}(r)$ = local speed of advance in off-design condition

$U_d(r)$ = local speed of advance at design condition

The values of $U_{od}(r)$ and the corresponding $a_{od}(r)$ are determined based on the assumption that the propeller operates in all conditions, design and off design, in the same disturbed fluid field responding with different propeller performance characteristics. The change of value of advance ratio at off-design condition is assumed due to change of speed of advance at constant RPM according to

$$\frac{[U_A(r)]_{od}}{[U_A(r)]_d} = \frac{[\bar{U}_A(r)]_{od}}{[\bar{U}_A(r)]_d} = \frac{J_{od}}{J_d}$$

from which

$$[U_A(r)]_{od} = \frac{J_{od}}{J_d} [U_A(r)]_d \tag{21}$$

where $U_A(r)$ and $\bar{U}_A(r)$ are the local speed of advance and its volumetric mean value, respectively. Then by making use of the definition of the advance ratio

$$a(r)_{od} = \frac{\Omega r_o}{[U_A(r)]_{od}} = \frac{\Omega r_o}{[U_A(r)]_d} \frac{J_d}{J_{od}}$$

the advance ratio at off-design condition is given by

$$a(r)_{od} = a(r)_d \frac{J_d}{J_{od}} \tag{22}$$

The normal velocity due to change of angle of attack at off-design condition ($\Delta J = J_{od} - J_d$) can now be determined. Then the additional blade loading $\Delta L^{(o)}_{od}$ is calculated through the integral equation (5).

4. Blade Pressure Distribution

The integral equation (5) can be solved successively by imposing boundary conditions given in Section 3 of the Analysis. Then the spanwise loading distribution is determined by

$$L^{(q)}(r) = \int_o^\pi L^{(q)}(r,\theta_\alpha) \sin\theta_\alpha \, d\theta_\alpha$$

$$= \int_o^\pi \sum_{\bar{n}=1}^{\bar{n}max} L^{(q,\bar{n})}(r) \, \Theta(\bar{n}) \sin\theta_\alpha d\theta_\alpha \tag{23}$$

For the unsteady loading due to wake ($q \neq o$), the complete Birnbaum series is used for the chordwise loading distribution. Thus

$$L^{(q)}(r) = \frac{1}{\pi} \int_o^\pi \left\{ L^{(q,1)}(r)(1+\cos\theta_\alpha) + \sum_{\bar{n}=2}^{n max} L^{(q,\bar{n})}(r) \sin(\bar{n}-1)\theta_\alpha \right.$$

$$\left. \sin\theta_\alpha \right\} d\theta_\alpha = L^{(q,1)}(r) + \tfrac{1}{2} L^{(q,2)}(r) \tag{24}$$

For the steady state loading due to ΔJ in the off-design condition the spanwise distribution is obtained by the first term of Eq. 24.

In the case of NACA-$\bar{a}$ mean line blade sections, with "roof-top" blade loading distribution:

$$L^{(o)}(r) = \begin{cases} L^{(0,1)}(r) & 0 \le \theta_\alpha \le \cos^{-1}(1 - 2\bar{a}) \\ L^{(0,1)}(r)\,\dfrac{1+\cos\theta_\alpha}{2(1-\bar{a})} & \cos^{-1}(1-2\bar{a}) \le \theta_\alpha \le \pi \end{cases}$$

The spanwise loading is given by

$$L^{(o)}(r) = L^{(0,1)}(r)\left\{ \int_o^\lambda \sin\theta_\alpha d\theta_\alpha + \frac{1}{2(1-\bar{a})} \int_\lambda^\pi (1+\cos\theta_\alpha)\sin\theta_\alpha d\theta_\alpha \right\}$$

$$= L^{(0,1)}(r)\,(\bar{a}+1) \qquad (25)$$

where

$$\lambda = \cos^{-1}(1 - 2\bar{a})$$

For any other arbitrary mean line, the spanwise loading distribution is derived from Equation (24) for $q = 0$

$$L^{(o,\bar{n})}(r) = \frac{1}{\pi} \int_o^\pi \left\{ L^{(0,1)}(r)(1+\cos\theta_\alpha) + \sum_{\bar{n}=2}^{nm\alpha x} L^{(o,\bar{n})}(r)\sin(\bar{n}-1)\theta_\alpha \sin\theta_\alpha \right\} d\theta_\alpha$$

$$= L^{(0,1)}(r) + \tfrac{1}{2} L^{(0,2)}(r) \qquad (26)$$

Whenever the cotangent Birnbaum mode is used, the Van Dyke or Lighthill correction[5,6] is applied to the chordwise pressure distribution to remove the physically unrealizable leading edge singularity.

Their simple rule for obtaining a uniformly valid solution is

$$\bar{C}_p = \frac{S}{S + \rho_o/2}\, C_p \qquad (27)$$

where

C_p = pressure coefficient according to first-order thin airfoil theory

S = chordwise location from the leading edge in fraction of chord length

ρ_o = leading edge radius of the profile in fraction of chord length

The modified chordwise loading distribution is then

$$L^{(q)}(r,\theta_\alpha) = \frac{1}{\pi}\left(\frac{1-\cos\theta_\alpha}{1+\rho_o-\cos\theta_\alpha}\right)\left\{L^{(q,1)}(r)\cot\frac{\theta_\alpha}{2} + \sum_{\bar{n}=2} L^{(q,\bar{n})}(r)\sin(\bar{n}-1)\theta_\alpha\right\} \tag{28}$$

Since the pressure near the leading edge is governed by the first term, the location of the maximum pressure near the leading edge is determined by

$$\frac{d}{d\theta_\alpha}\left(\frac{\sin\theta_\alpha}{1+\rho_o-\cos\theta_\alpha}\right) = 0$$

which yields

$$\cos\theta_\alpha = \frac{1}{1+\rho_o}$$

This is the chordwise location of a point where the maximum pressure near the leading edge will occur after the application of the leading edge correction, provided $\rho_o < .015$, otherwise the sine series will influence the location of maximum pressure near the leading edge.

ITERATIVE PROCEDURE

As was noted earlier, a propeller operating behind a hull is subjected to the effect of a hull wake of varying intensity (weak to strong) and it is also influenced by its self-induction. The former can be taken into account by a harmonic analysis of the wake, as has been done before; the latter, self-induction, however, depends on a priori knowledge of the propeller loading which requires that the reference surface be established in advance.

The harmonic content of the wake based on the local speed of advance is used as the inflow to the propeller. The wake intensities may be quite strong and even of the same order of magnitude as the free stream velocity (ship speed). These velocities cannot be considered as perturbations and, thus, a strictly linearized theory is no longer valid. Second-order terms cannot be ignored as small quantities. However, second order theory (nonlinear theory) cannot be easily developed so as to lead to a manageable numerical approach. An iterative procedure is established based on a combination of the nonlinear form of the Bernoulli equation with a kinematic boundary condition existing at the designed operational condition for the selection of the reference helicoidal surface around which a perturbation theory will be developed. A flow field closer to the propeller operating condition is achieved and thus the requirement of the small perturbation quantities will be reinforced. This approach is applicable to moderately to heavily loaded propellers immersed in a strong wake.

1) The Bernoulli Equation

For a moderately loaded propeller operating in a steady inflow field whose velocity components in the axial, tangential and radial directions are given by

$$U_A(r) + \frac{\partial \Phi_o}{\partial x} \quad , \quad r\Omega + V_T - \frac{1}{r}\frac{\partial \Phi_o}{\partial \varphi} \quad , \quad W_r + \frac{\partial \Phi_o}{\partial r}$$

respectively, the Bernoulli equation for a point (x,r,φ) in the field becomes

$$\frac{p_o(x,r,\varphi)}{\rho_f} + \frac{1}{2}\left[\left(U_A + \frac{\partial \Phi_o}{\partial x}\right)^2 + \left(r\Omega + V_T - \frac{1}{r}\frac{\partial \Phi_o}{\partial \varphi}\right)^2 + \left(W_r + \frac{\partial \Phi_o}{\partial r}\right)^2\right]$$

$$= \frac{p_\infty}{\rho_f} + \frac{1}{2}\left[U_A^2 + \left(r\Omega + V_T\right)^2 + W_R^2\right] \qquad (29)$$

where

p_o is the mean local pressure

U_A = local speed of advance

Φ_o = the flow velocity potential function

and V_T and W_R = mean wake velocity in the tangential and radial directions, respectively.

The rest of the symbols are as defined previously.

It is assumed that for mean ship wake flow

$$\bar{V}_T = 0 \text{ (always true for a single screw)}$$

and $$\bar{W}_R = 0 \quad \text{and} \quad \frac{\partial \Phi_o}{\partial r} = 0 \text{ (no radial variation is taken into account)}$$

and reference pressure $p_\infty = 0$.

Thus, Eq.(29) yields

$$\left[U_A \frac{\partial \Phi_o}{\partial x} + \frac{1}{2}\left(\frac{\partial \Phi_o}{\partial x}\right)^2\right] + \left[-r\Omega \frac{1}{r} \frac{\partial \Phi_o}{\partial \varphi} + \frac{1}{2}\left(\frac{1}{r} \frac{\partial \Phi_o}{\partial \varphi}\right)^2\right] = - \frac{p_o}{\rho_f} (x,r,\varphi)$$

which includes the second order terms, or

$$\left[U_A + \frac{1}{2}\left(\frac{\partial \Phi_o}{\partial x}\right)\right] \frac{\partial \Phi_o}{\partial x} - \left[r\Omega - \frac{1}{2}\left(\frac{1}{r} \frac{\partial \Phi_o}{\partial \varphi}\right)\right] \frac{1}{r} \frac{\partial \Phi_o}{\partial \varphi} = - \frac{p_o}{\rho_f} (x,r,\varphi) \tag{30}$$

For a coordinate system fixed in space and for a right-handed propeller rotating with angular velocity Ω,

$$\varphi = -\Omega t \, .$$

Thus, the above equation becomes

$$\left[U_A + \frac{1}{2}\left(\frac{\partial \Phi_o}{\partial x}\right)\right] \frac{\partial \Phi_o}{\partial x} + \left[r\Omega - \frac{1}{2} \frac{1}{r} \frac{\partial \Phi_o}{\partial \varphi}\right] \frac{1}{r\Omega} \left(\frac{\partial \Phi_o}{\partial t}\right) = - \frac{p_o}{\rho_f} (x,r,\varphi) \tag{31}$$

Letting

$$\begin{aligned} A(x,r,\varphi) &= U_A + \frac{1}{2} \left(\frac{\partial \Phi_o}{\partial x}\right) \\ B(x,r,\varphi) &= \frac{1}{r\Omega} \left[r\Omega - \frac{1}{2}\left(\frac{1}{r} \frac{\partial \Phi_o}{\partial \varphi}\right)\right] \end{aligned} \tag{32}$$

Eq.(31) is written as

$$A \frac{\partial \Phi_o}{\partial x} + B \frac{\partial \Phi_o}{\partial t} - \frac{p_o}{\rho_f}(x,r;t) = \psi(x,r;t) \tag{33}$$

where

$$\psi(x,r;t) = -\frac{p_o(x,r;t)}{\rho_f} = \text{acceleration potential function.}$$

The formal solution of the differential Eq.(33) is obtained by the method of characteristics provided the coefficients A and B are known constants.

This present scheme is also used as a means to introduce the propeller induction. Identifying the propeller-induced velocity in the axial and tangential directions by

$$\frac{\partial \Phi_o}{\partial x} = u_i(x,r;t)$$

and

$$-\frac{1}{r}\frac{\partial \Phi_o}{\partial \varphi} = v_i(x,r;t)$$

respectively, the coefficients of differential equation (33) become:

$$\begin{aligned} A(x,r;t) &= U_A + \frac{1}{2} u_i \\ B(x,r;t) &= \frac{1}{r\Omega}\left[r\Omega + \frac{1}{2} v_i\right] \end{aligned} \tag{34}$$

These induced velocities can now be approximately evaluated by taking one-half of the corresponding values at infinity (well-known results from the momentum theory). The steady induced velocities in the far field can easily be calculated once the propeller loading is known. In fact, in Reference 7 it is shown that the steady axial velocity at $x \to \infty$ in uniform flow is given by

$$u_i = \frac{-N}{2\pi\rho_f U r_o} \sum_{\bar{n}=1}^{\max \bar{n}} \frac{\Lambda(\bar{n})_{(0)} L(0,\bar{n})(r)}{r} \tag{35}$$

where all the symbols are as previously defined and linear dimensions are non-dimensionalized with respect to propeller radius.

It can be further shown[7] that the steady tangential velocity in the far

field can be expressed in terms of the axial induced velocity by

$$v_i(x,r;t) = -\frac{1}{ar}\, u_i(x,r;t)$$

thus the coefficients (Eq.34) become:

$$\begin{aligned} A(x,r;t) &= U_A + \frac{1}{2}\, u_i(x,r;t) \\ B(x,r;t) &= \frac{1}{r\Omega}\left[r\Omega - \frac{1}{2}\,\frac{u_i(x,r;t)}{ar}\right] \end{aligned} \tag{36}$$

which incorporate the propeller speed of advance and the propeller induction, both of which are considered to vary radially.

As will be seen later, once the potential function $\Phi_o(x,r;t)$ is determined at a stage of the development, the blade loadings can be evaluated and hence the propeller induction effects as well as any other flow characteristics can be calculated. The coefficients given by Eq.(36) are considered to be known at that stage, and hence the differential equation

$$A(x,r;t)\,\frac{\partial \Phi_o}{\partial x} + B(x,r;t)\,\frac{\partial \Phi_o}{\partial t} = \Psi(x,r;t) \tag{37}$$

(see Eq.33) can now be solved by the method of characteristics provided that A and B are determined at $x=0$ (at the propeller plane), i.e., they are specifiable constants. The characteristics are deduced from

$$\frac{dx}{A} = \frac{dt}{B}$$

which, upon integration, yields

$$Bx - At = \text{constant}$$

Letting

$$\begin{aligned} \xi &= Bx - At \\ \eta &= x \end{aligned} \tag{38}$$

then

$$\frac{\partial}{\partial x} = \xi_x \frac{\partial}{\partial \xi} + \eta_x \frac{\partial}{\partial \eta} = B\,\frac{\partial}{\partial \xi} + \frac{\partial}{\partial \eta}$$

$$\frac{\partial}{\partial t} = \xi_t \frac{\partial}{\partial \xi} + \eta_t \frac{\partial}{\partial \eta} = -A\,\frac{\partial}{\partial \xi}$$

Multiplying the above relations by A and B, respectively, and substituting

the results into Eq.(37) yields

$$A \frac{\partial \Phi_o}{\partial \eta} = \psi[\eta, r; \frac{1}{A}(B\eta - \xi)]$$

which upon integration becomes

$$\Phi_o(x,r;t) = \frac{1}{A} \int_{-\infty}^{x} \psi[\tau, r; \frac{1}{A}(B\tau - \xi)]d\tau$$

Making use of the relations given by Eq.(38), the above solution can be written as

$$\Phi_o(x,r;t) = \frac{1}{A} \int_{-\infty}^{x} \psi[\tau, r; t - \frac{B}{A}(x-\tau)]d\tau \tag{39}$$

This is of the same structure as the existing relation between the velocity and acceleration potentials for the case of a lightly loaded propeller, which was the subject of the previous study.[2]

The above relation indicates that the solution $\Phi_o(x,r;t)$ for the velocity potential is obtained through the so-called "History Integral" of the corresponding acceleration potential where the time is shifted by the amount $\frac{B}{A}(x-\tau)$. Thus, the term involving the "time element" becomes

$$\Omega\left[t - \frac{B}{A}(x-\tau)\right] = \Omega t - \frac{r_o r \Omega - \frac{1}{2}\frac{u_i(x,r;t)}{ar}}{r\left[U_A + \frac{1}{2}u_i(x,r;t)\right]}(x-\tau) \tag{40}$$

where all the linear quantities are expressed in a non-dimensional form in terms of the propeller radius r_o. Thus, the "inverse advance ratio" $ar = \frac{\Omega r}{U}$ which was introduced in the study of the lightly loaded propeller[2] is defined in the present study by

$$a_e r = \frac{\Omega r_o r - \frac{1}{2}\frac{u_i}{ar}}{U_A + \frac{1}{2}u_i} \tag{41}$$

which will be called an "effective inverse advance ratio".

It is shown, therefore, that the present problem with propeller exposed to the advance speed and influenced by its self-induction admits of the same formal solution as in reference 2. The same mechanics can be utilized as before, provided the coefficients of the differential Eq.(33) are known. This can be achieved by introducing an iterative procedure.

2) Iterations

At first it is assumed that the induction effects are omitted (i.e., $u_i^{(1)}=0$, $v_i^{(1)}=0$), so that the coefficients A(x,r;t) and B(x,r;t) become

$$A^{(1)}(0,r;t) = U_A(r)$$

$$B^{(1)} = 1$$

both known quantities, in which case the solution yields

$$\Phi^{(1)}(x,r;t) = \frac{1}{U_A} \int_{-\infty}^{x} \psi^{(1)} \left(\tau, r; t - \frac{x-\tau}{U}\right) d\tau$$

which is identical to that of a "lightly loaded" propeller[2] except that the present solution incorporates a radial variation in the inflow field. The variation does not introduce any additional complication since the problem is solved by dividing the lifting surface into radial strips with specified inflow field at each radius.

Knowing the velocity potential $\Phi^{(1)}(x,r;t)$ and the "effective inverse advance ratio" $a_e^{(1)} = \frac{\Omega}{U_A} = \frac{2\pi n}{U_A}$ (n = the propeller RPS, and $a_e^{(1)} = a$), through the existing 'machinery' (analysis and program) the steady state blade loading $L_{(1)}^{(0,\bar{n})}(r)$ is determined (subscript refers to the order of iteration). Then the induction effects $u_i^{(2)}(0,r;t)$ are calculated through Eq.(35). A new set of coefficients $A^{(2)}(0,r;t)$ and $B^{(2)}(0,r;t)$ are determined through Eq.(36).

With these new coefficients, a new solution $\Phi_o^{(2)}(x,r;t)$ is established:

$$\Phi_o^{(2)}(x,r;t) = \frac{1}{A^{(2)}} \int_{-\infty}^{x} \psi^{(2)} \left(\tau, r; t - \frac{B^{(2)}}{A^{(2)}} (x-\tau)\right) d\tau$$

With "effective inverse advance ratio"

$$a_e^{(2)}{}_r = \frac{\Omega r_o r - \frac{1}{2} \frac{u_i^{(2)}}{a_e^{(1)}{}_r}}{U_A + \frac{1}{2} u_i^{(2)}}$$

the new loading $L_{(2)}^{(0,\bar{n})}(r)$ and inductions $u_i^{(3)}$ are calculated, and thus

establish the new coefficients $A^{(3)}(0,r;t)$ and $B^{(3)}(0,r;t)$. At that stage the new iteration begins.

The results of the j^{th} iteration are presented in the following table:

Coefficients $\quad A^{(j)} = U_A + \frac{1}{2} u_i^{(j)} \qquad B^{(j)} = \left[\Omega r_o r - \frac{1}{2} \frac{u_i^{(j)}}{a_e^{(j-1)} r} \right] \frac{1}{\Omega r_o r}$

"Effective inverse advance coefficient"
$$a_e^{(j)} = \frac{\Omega r r_o - \frac{1}{2} a_e^{(j-1)} r \, u_i^{(j)}}{r \left[U_A + \frac{1}{2} u_i^{(j)} \right]} = \frac{a_e^{(1)} r - \frac{1}{2 a_e^{(j-1)} r} \frac{u_i^{(j)}}{U_A}}{r \left[1 + \frac{u_i^{(j)}}{2 U_A} \right]}$$

Solution of d.e.
$$\Phi^{(j)}(x,r;t) = \frac{1}{A^{(j)}} \int_{-\infty}^{x} \psi^{(j)} \left[\tau, r; t - \frac{B^{(j)}}{A^{(j)}} (x-\tau) \right] d\tau$$

Steady-Induction
$$u_i^{(j)} = \frac{-N}{2\pi \rho_f U r_o} \sum_{\bar{n}=1}^{\max \bar{n}} \frac{\Lambda^{(\bar{n})}(0) L^{(0,\bar{n})}_{(j-1)}(r)}{r}$$

This iterative procedure will continue until the potential function $\Phi^{(j)}(x,r;t)$ or, more conveniently, the "effective inverse advance coefficient" $a_e^{(j)}$, does not vary in two consecutive iterations. With the final value of $a_e^{(j)}$, the reference helicoidal surface is established and this will be used as the basic information for the calculations of the steady and unsteady blade loading and hydrodynamic forces and moments.

It is clear that the number of required iterations depend to a great extent on how close the initial value of the "effective inverse advance coefficient" $a_e^{(1)}$ is to its final value. A simplified procedure is given below.

It is known that the pitch of a well designed "wake-adapted propeller" nearly satisfies the following "kinematic condition"

$$U_A + u_i = (\Omega r + v_i)\tan\theta_p$$

$$= (\Omega r - \frac{u_i}{ar})\tan\theta_p$$

from which the axial induction is

$$u_i = (\Omega r \tan\theta_p - U_A)\frac{ar}{ar + \tan\theta_p} \tag{42}$$

where θ_p is the propeller pitch angle.

From Eq.(41) the axial induction is determined as

$$u_i = 2(r\Omega - arU_A)\frac{ar}{1 + a^2r^2} \tag{43}$$

which is considered to be the result of the "dynamic condition" since Eq.(41) is derived from the Bernoulli equation.

Combining the "kinematic" (Eq.42) and "dynamic" (Eq.43) conditions, yields

$$E\,a^2r^2 - 2D\,ar - E = 0 \tag{44}$$

whose solution leads to

$$ar = \frac{D + \sqrt{D^2+E^2}}{E} \tag{45}$$

where

$$D = \Omega r - U_A \tan\theta_p$$

$$E = \Omega r \tan\theta_p + U_A$$

With the initial value of a_e obtained from Eq.(45), the iterative procedure, described above, starts. It is seen from the numerical calculations that this approach has reduced the number of iterations considerably, by 50 percent.

Once the reference helicoidal surface is established and the "effective inverse advance coefficient" a_e is determined, the numerical procedure becomes identical to that developed previously in Reference 2 for the steady and unsteady flow conditions.

PRESSURES, HYDRODYNAMIC FORCES AND MOMENTS, AND BLADE BENDING MOMENTS

1) Blade Pressure Distribution on Each Blade Face

In the preceding sections the pressure difference $\Delta p^{(q)}(r)$, at a given radial position r and frequency q, between back (suction) and front (pressure) faces of the blade surface is determined. On the suction side of the pressure due to loading is $+\Delta p^{(q)}(r)/2$; on the pressure side it is $-\Delta p^{(q)}(r)/2$.

In addition, a non-lifting pressure P_T is generated due to the symmetrical "flow distortion" thickness effect which will be present only in the steady state since the blade is considered to be rigid. P_T is derived in Appendix C by means of the "thin body" approximation (see Reference 8).

The instantaneous pressure is the sum of the blade pressures due to all frequencies contributing significantly. On the pressure or suction face, when the blade swings around its shaft in the clockwise direction from its upright position (12M), it is

$$P_{p,s}(r) = \mathrm{Re} \sum_{q=o} P^{(q)}_{p,s}(r)\, e^{-iq\Theta} = \sum_{q=o} |P^{(q)}_{p,s}(r)| \cos(q\Theta - \varphi_q) \qquad (46)$$

where

$$\varphi_q = \text{phase angle} = \tan^{-1} \frac{(P^{(q)}_{p,s})_{Im}}{(P^{(q)}_{p,s})_{Re}}$$

(the subscripts Re and Im indicate the real and imaginary parts) and Θ is blade angular position, positive in the counterclockwise direction as is φ_q.

2) Propeller-Generated Forces and Moments

The principal components of the hydrodynamic forces and moments are shown in Figure 2 with the sign convention adopted. The total forces at frequency $\ell N(\ell=0,1,2,\ldots)$ induced by an N-bladed propeller are determined as (see Reference 2):

$$F_x = \mathrm{Re}\{Nr_o\, e^{i\ell N\Omega t} \int_o^1 L^{(\ell N)}(r)\cos\theta_p(r)dr\}$$

$$F_y = \mathrm{Re}\{\frac{Nr_o}{2} e^{i\ell N\Omega t} \int_o^1 \sum_{\bar{n}=1} [L^{(\ell N-1,\bar{n})}(r)\Lambda^{(\bar{n})}(-\theta_b^r) + L^{(\ell N+1,\bar{n})}(r)\Lambda^{(\bar{n})}(\theta_b^r)]$$
$$\sin\theta_p(r)dr\}$$

$$F_z = \mathrm{Re}\{\frac{-Nr_o}{2i} e^{i\ell N\Omega t} \int_o^1 \sum_{\bar{n}=1} [L^{(\ell N-1,\bar{n})}(r)\Lambda^{(\bar{n})}(-\theta_b^r) - L^{(\ell N+1,\bar{n})}(r)\Lambda^{(\bar{n})}(\theta_b^r)]$$
$$\sin\theta_p(r)dr\} \qquad (47a)$$

The moments are determined by:

$$Q_x = -\mathrm{Re}\{Nr_o^2\, e^{i\ell N\Omega t} \int_o^1 L^{(\ell N)}(r)\sin\theta_p(r)rdr\}$$

$$Q_y = \mathrm{Re}\{\frac{Nr_o^2}{2} e^{i\ell N\Omega t} \int_o^1 \{\sum_{\bar{n}=1} [L^{(\ell N-1,\bar{n})}(r)\Lambda^{(\bar{n})}(-\theta_b^r) + L^{(\ell N+1,\bar{n})}(r)\Lambda^{(\bar{n})}(\theta_b^r)]\cos\theta_p(r)$$
$$+ \sum_{\bar{n}=1} [L^{(\ell N-1,\bar{n})}(r)\Lambda_1^{(\bar{n})}(-\theta_b^r) - L^{(\ell N+1,\bar{n})}(r)\Lambda_1^{(\bar{n})}(\theta_b^r)](i\theta_b^r)\sin\theta_p(r)\tan\theta_p(r)\}rdr\}$$

$$Q_z = \mathrm{Re}\{\frac{-Nr_o^2}{2i} e^{i\ell N\Omega t} \int_o^1 \{\sum_{\bar{n}=1} [L^{(\ell N-1,\bar{n})}(r)\Lambda^{(\bar{n})}(-\theta_b^r) - L^{(\ell N+1,\bar{n})}(r)\Lambda^{(\bar{n})}(\theta_b^r)]\cos\theta_p(r)$$
$$+ \sum_{\bar{n}=1} [L^{(\ell N-1,\bar{n})}(r)\Lambda_1^{(\bar{n})}(-\theta_b^r) + L^{(\ell N+1,\bar{n})}(r)\Lambda_1^{(\bar{n})}(\theta_b^r)](i\theta_b^r)\sin\theta_p(r)\tan\theta_p(r)\}rdr\} \qquad (47b)$$

where $\Lambda^{(\bar{n})}(z)$ and $\Lambda_1^{(\bar{n})}(z)$ are as defined in Appendix A.

It is seen from Eqs. (47a,b) that the transverse bearing forces and bending moments are evaluated from propeller loading components $L^{(q,\bar{n})}(r)$ associated with wake harmonics at frequencies adjacent to blade frequency, i.e. at $q = \ell N \pm 1$, whereas the thrust and torque are determined from the

loading $L^{(q)}(r)$ at blade frequency $q=\ell N$. At $\ell=0$ (steady-state), the mean transverse forces and bending moments are determined at shaft frequency. Thus:

$$\bar{F}_y = \text{Re}\left\{\frac{Nr_o}{2}\int_o^1 \left[\sum_{\bar{n}=1} L^{(1,\bar{n})}(r)\Lambda^{(\bar{n})}(\theta_b^r)\right]\sin\theta_p(r)dr\right\}$$

$$\bar{F}_z = \text{Re}\left\{\frac{Nr_o}{2i}\int_o^1 \left[\sum_{\bar{n}=1} L^{(1,\bar{n})}(r)\Lambda^{(\bar{n})}(\theta_b^r)\right]\sin\theta_p(r)dr\right\}$$

$$\bar{Q}_y = \text{Re}\left\{\frac{Nr_o^2}{2}\int_o^1 \left\{\left[\sum_{\bar{n}=1} L^{(1,\bar{n})}(r)\Lambda^{(\bar{n})}(\theta_b^r)\cos\theta_p(r) - \left[\sum_{\bar{n}=1} L^{(1,\bar{n})}(r)\Lambda_1^{(\bar{n})}(\theta_b^r)\right](i\theta_b^r)\sin\theta_p(r)\tan\theta_p(r)\right\}rdr\right\}$$

$$\bar{Q}_z = \text{Re}\left\{\frac{NR_o^2}{2i}\int_o^1 \left\{\left[\sum_{\bar{n}=1} L^{(1,\bar{n})}(r)\Lambda^{(\bar{n})}(\theta_b^r)\cos\theta_p(r) - \left[\sum_{\bar{n}=1} L^{(1,\bar{n})}(r)\Lambda_1^{(\bar{n})}(\theta_b^r)\right](i\theta_b^r)\sin\theta_p(r)\tan\theta_p(r)\right\}rdr\right\} \qquad (47c)$$

All forces and moments can be written in the form

$$R_e[C^{(q)}e^{i\varphi_q}e^{-iq\Theta}] = C^{(q)}\cos(-q\Theta+\varphi_q) = C^{(q)}\cos(q\Theta-\varphi_q)$$

where Θ is blade angular position, *positive in the counter-clockwise direction* from zero at the upright position (12M), q is order of shaft frequency, $C^{(q)}$ is magnitude of force or moment, and φ_q is phase angle (electrical) determined as the angle whose tangent is the imaginary part (sine part) over the real part (cosine part). (The program output gives $C^{(q)}$ and φ_q.)

When φ_q is positive, the peak (or trough) of $C^{(q)}$ is to the left of the upright position, i.e., leads; when φ_q is negative, the peak (or trough) is to the right of the upright position and lags that of input.

In Reference 2, as a first attempt at estimating the frictional contribution to thrust F_x and torque Q_x, use was made of the Prandtl-Schlichting formula for the friction coefficient for one side of a smooth flat plate as was suggested by Hoerner.[9] The present study follows Reference 2 in this matter with this exception: in the formulas for friction coefficient and frictional thrust and torque, the inverse advance ratio is no longer $a = \Omega r_o/U$, based on forward speed of the ship and constant over the propeller span, but $a_A(r) = \Omega r/U_A(r)$, based on local speed of advance and varying with radial position.

3) Blade Bending Moments

The blade bending moment about the face pitch line at any radius r_j of a blade is calculated from the chordwise integrated loading (spanwise component) $L^{(q)}(r)$ at any shaft frequency q as

$$M_b^{(q)} e^{iq\Omega t} = r_o^2 e^{iq\Omega t} \int_{r_j}^{1} L^{(q)}(r) \cos [\theta_p(r) - \theta_p(r_j)] (r - r_j) dr \qquad (48)$$

The positive blade bending moment about the face pitch line is that which puts the face of the blade in compression.

The instantaneous blade bending moment distribution when the propeller swings around its shaft in the clockwise direction is

$$M_b = R_e \sum_q M_b^q e^{-iq\theta} = \sum_q |M_b^q| \cos(q\theta - \varphi_q) \qquad (49)$$

where φ_q is the phase angle (electrical).

It should be noted that in the program the value of r_j of Eq.(48) is limited to any of the midpoints of the radial strips into which the blade span is divided, at which points the pitch angles, as well as other geometrical characteristics, are given as input. The bending moment at any other radial position can be obtained by interpolation or extrapolation.

NUMERICAL RESULTS

The theoretical approach developed in the preceding sections for the evaluation of the blade pressure distributions due to loading and thickness effects and of the resulting forces and moments has been adapted to a high-speed digital computer (CDC-6600 or Cyber 176).

The numerical procedure has been applied to propellers of different loading from light to moderate to heavy:

a) the DTNSRDC Propeller 4118 tested at DTNSRDC [10,11] in screen wakes (3-cycle and 4-cycle screens)

b) the Sharp Propeller V-3275 in the wake of ship model 4986 (S.S. MICHIGAN), the wake survey and propeller geometry supplied by the U.S. Maritime Administration

c) the NSMB Propeller 4930 in the wake of ship model 4705, the wake survey and propeller geometry supplied by Lloyd's Register of Shipping

The particulars are listed in Table 1.

TABLE 1

Propeller Designation	DTNSRDC 4118	SHARP V-3275	NSMB 4930
Expanded Area Ratio, EAR	0.60	0.564	0.810
Pitch-Diameter Ratio, P/D at 0.7 Radius	1.077	1.080	0.757
Skew, deg	0	11.5	30.0
Diameter, D, ft	1.0	22.5	6.837
No. of Blades, N	3	5	5
NACA $\bar{a}$ Meanline Section	$\bar{a} = 0.8$	$\bar{a} = 0.4$	$\bar{a} = 0.7$
RPM (= 60n)	900	106	213.6
Advance Ratio, J = U/nD	0.831	0.993	0.746
Free Stream Velocity, U, ft/sec	12.465	39.50	18.158
Speed of Advance, U_A, at 0.7 Radius, ft/sec	12.81	33.18	9.02

Relevant geometric characteristics of the 3 propellers, namely, the ratios of maximum camber to chord length, m_x/c, of maximum thickness to chord, t_o/c, of leading edge radius to chord, ρ_o, of chord/diameter, c/D, and of pitch to diameter, P/D, are given in Tables 2-4.

TABLE 2. DTNSRDC PROPELLER 4118

Radius	m_x/c	t_o/c	ρ_o	c/D	P/D
0.25	0.0228	0.090	0.00525	0.347	1.085
0.35	0.0231	0.068	0.00290	0.386	1.083
0.45	0.0224	0.052	0.00170	0.425	1.081
0.55	0.0212	0.040	0.00100	0.454	1.079
0.65	0.0203	0.031	0.00060	0.464	1.077
0.75	0.0198	0.024	0.00035	0.452	1.076
0.85	0.0189	0.018	0.00025	0.405	1.074
0.95	0.0174	0.016	0.00020	0.278	1.072

TABLE 3: SHARP PROPELLER V-3275

0.25	0.0553	0.232	0.059	0.166	1.000
0.35	0.0445	0.166	0.030	0.200	1.032
0.45	0.0374	0.122	0.016	0.231	1.055
0.55	0.0321	0.094	0.0097	0.251	1.083
0.65	0.0268	0.073	0.0059	0.260	1.080
0.75	0.0218	0.056	0.0035	0.257	1.079
0.85	0.0174	0.042	0.0019	0.236	1.073
0.95	0.0138	0.031	0.0011	0.168	1.057

TABLE 4. NSMB PROPELLER 4930

0.232	0.0304	0.168	0.04087	0.234	0.729
0.335	0.0288	0.124	0.02238	0.268	0.750
0.437	0.0279	0.088	0.01210	0.308	0.754
0.539	0.0258	0.065	0.00680	0.343	0.758
0.642	0.0217	0.049	0.00309	0.364	0.759
0.744	0.0178	0.039	0.00183	0.366	0.754
0.847	0.0138	0.030	0.00162	0.343	0.741
0.949	0.0101	0.023	0.00175	0.264	0.724

Mean wake information is presented in Table 5 as the ratio of speed of advance, U_A, to the free stream velocity, U, at 8 equidistant radial positions between propeller hub and tip (see Tables 2-4).

TABLE 5. U_A/U - RATIO OF SPEED OF ADVANCE TO FREE STREAM VELOCITY

Propeller Wake U, ft/sec	DTNSRDC 4118 Screen 12.465	SHARP V-3275 Model 4986 39.50	NSMB 4930 Model 4705 18.158
Radial Position	U_A/U	U_A/U	U_A/U
1	0.970	0.599	0.207
2	0.969	0.678	0.285
3	0.984	0.747	0.354
4	1.009	0.800	0.407
5	1.026	0.829	0.452
6	1.028	0.844	0.527
7	1.026	0.848	0.655
8	1.025	0.852	0.791

DTNSRDC Propeller 4118

Results of calculations of the hydrodynamic forces and moments by the present approach, as implemented by the PLEXVAN program, are presented in Table 6 for the 3-bladed propeller 4118. The steady and blade-frequency K coefficients are compared there with available experimental values,[10] and with values obtained through the approach of Reference 2 by the PPEXACT modified code.*

*Since the publication of Reference 2 the numerical procedure of the PPEXACT program has been modified for greater accuracy of the chordwise distributions.

TABLE 6

DTNSRDC PROPELLER 4118
IN 3-CYCLE AND 4-CYCLE SCREEN WAKES

Coefficient	CALCULATIONS PLEXVAN Program Mag.	PLEXVAN Program Phase deg	CALCULATIONS PPEXACT Program Mag.	PPEXACT Program Phase deg	EXPERIMENTAL Measurements Mag.	EXPERIMENTAL Measurements Phase deg
Mean						
$\bar{K}_T$	0.166	180	0.166	180	0.154	180
$\bar{K}_Q$	0.0324	0	0.0323	0	0.0290	0
Blade Frequency						
$\tilde{K}_T$	0.0735	- 22.9	0.0742	- 23.4	0.0685	-32
$\tilde{K}_Q$	0.0126	157.2	0.0127	156.6	0.0102	135
$\tilde{K}_{F_y}$	0.0175	- 8.3	0.0162	- 8.9	0.0139	30
$\tilde{K}_{Q_y}$	0.0124	- 24.5	0.0114	- 25.0	0.0109	30
$\tilde{K}_{F_z}$	0.0175	- 98.3	0.0162	- 98.9	0.0131	-67
$\tilde{K}_{Q_z}$	0.0124	-114.5	0.0114	-115.0	0.0114	-67

Comparisons between the results of the two theoretical approaches for the chordwise and spanwise distributions of pressure are graphically exhibited in Figures 2 to 4.

It is seen that for this lightly loaded propeller with $C_T = 8\bar{K}_T/\pi J_A^2$ approximately 0.6, there are only slight differences between the present approach and that of Reference 2, as was expected.

Sharp Propeller V-3275

Similar calculations have been performed for the Sharp 5-bladed propeller V-3275. The results are shown in Table 7 and graphically in Figures 5-8. Also tabulated are some results obtained from Troost B-5 propeller charts.

TABLE 7. SHARP PROPELLER V-3275 IN THE WAKE OF THE S.S. MICHIGAN

	CALCULATIONS				
	PLEXVAN Program		PPEXACT Program		TROOST B-5 Prop.*
Coefficient	Mag.	Phase deg	Mag.	Phase deg	Mag.
Mean					
$\bar{K}_T$	0.222	180	0.226	180	0.185
$\bar{K}_Q$	0.0400	0	0.0408	0	0.0325
$\bar{K}_{F_y}$	0.0159	180	0.0171	180	
$\bar{K}_{Q_y}$	0.0111	180	0.0118	180	
$\bar{K}_{F_z}$	0.0144	0	0.0159	0	
$\bar{K}_{Q_z}$	0.00983	0	0.0103	0	
Blade Frequency					
$\tilde{K}_T$	0.00635	177.8	0.00638	166.9	
$\tilde{K}_Q$	0.00108	- 2.1	0.00106	- 12.9	
$\tilde{K}_{F_y}$	0.01265	-140.8	0.01171	-143.1	
$\tilde{K}_{Q_y}$	0.00842	-153.1	0.00777	-152.5	
$\tilde{K}_{F_z}$	0.00442	- 75.2	0.00437	- 76.1	
$\tilde{K}_{Q_z}$	0.00274	- 74.7	0.00272	- 73.2	

*at $J_A = U_A/nD$ at 0.7 radius

In this case, $C_T = 8\,\bar{K}_T/\pi J_A^2$ is approximately 0.8. It is seen that the hydrodynamic force and moment results of the present analytical approach differ slightly from those of the PPEXACT modified program. The blade pressure distribution of Figures 7 and 8 show larger differences between the two methods.

NSMB Propeller 4930

A comparison of results of the PPEXACT and PLEXVAN programs for this 5-bladed propeller is presented in Table 8 and Figures 9 to 11. The computations were performed for the steady-state case, q=0, only, since just the mean wake velocity was supplied.

Both Davidson Laboratory sets of calculations were compared with the results of the NSMB lifting-surface program which were provided in the form of graphs of spanwise load distribution and chordwise pressure distribution. The values of mean thrust, $\bar{K}_T$, and torque, $\bar{K}_Q$, coefficients shown in Table 8 for the NSMB program are derived from the spanwise loads.

This propeller with a $C_T \approx 4$ is more heavily loaded than the other two propellers and the results show larger differences when the two theoretical approaches are compared.

TABLE 8. NSMB PROPELLER 4930 IN THE WAKE OF MODEL 4705

Mean Coefficient	CALCULATIONS PLEXVAN	PPEXACT	NSMB	TROOST B-5 PROP*
$\bar{K}_T$	-0.202	-0.216	-0.227	-0.20
$\bar{K}_Q$	0.0272	0.0294	0.0305	0.026

*at $J_A = U_A/nD$ at 0.7 radius.

CONCLUSIONS

A theory and corresponding computer program have been developed for a marine propeller operating in non-uniform inflow by taking into account the radially varying mean wake and mean propeller induction.

The helicoidal reference surface of radially varying pitch is established through an iterative procedure by combining the non-linear form of the Bernoulli equation with an appropriate kinematic condition existing at the design stage.

The numerical procedure furnishes information on the blade pressure distribution, as well as the resulting hydrodynamic forces and moments in the steady and unsteady flow conditions. The approach is valid for moderately to heavily loaded propellers.

It is seen from this small number of calculations for propellers with thrust coefficient C_T varying between 0.6 and 4.0 that the differences between steady and unsteady forces and moments calculated by the present theory (coded as PLEXVAN) and the corresponding values determined by the previous approach (coded as PPEXACT) are larger as C_T increases. However, the differences between the results of both procedures are minor even for the propeller operating under more heavily loaded conditions.

The PPEXACT method assumes the reference surface (along which the shed vorticity is considered to be convected) to be a pure helicoid whose local pitch is fixed by the joint action of the forward ship speed and the blade tangential velocity at any radius. The difference between the ship speed and the radially varying wake speed is taken as a perturbation from this surface. On the other hand, in the present (PLEXVAN) method to begin with the reference surface (based on the non-linear form of the Bernoulli equation) takes into account the radially varying mean wake and mean propeller induction.

It would appear that the two methods yield comparable results provided that the prescribed procedures are closely adhered to (e.g., in the PPEXACT method the hydrodynamic pitch $\tan^{-1}(U/r\Omega)$ must use U = ship speed). The advantage of the PPEXACT program lies in its considerable saving of computer time.

If, however, greater accuracy in the evaluation of hydrodynamic forces and moments is required and more precise blade pressure is needed, then the program PLEXVAN must be exercised.

In the analysis performed in Reference 12 to evaluate the sensitivity of various wake parameters, the hydrodynamic pitch angle β was found to be the most critical one. A set of calculations for propellers with 36° skewness indicates that a decrease in β of 10° results in a decrement of approximately 18% in K_T (see Figure 11 of Reference 12). On the other hand, the present calculations for the NSMB 4930 propeller with 30° skew indicate that with a decrease in β of 4.5°, there is a decrement of approximately 7% in K_T. The trend is shown in both cases to be about the same. For a final assessment, more systematic calculations must be performed and compared with corresponding measurements.

ACKNOWLEDGMENT

The authors wish to express their appreciation to Mr. Ping Liao for reviewing and executing the program.

REFERENCES

1. Tsakonas, S., Jacobs, W.R., and Ali, M.R., "Exact Linear Lifting-Surface Theory for a Marine Propeller in a Nonuniform Flow Field," Davidson Laboratory Report 1509, Stevens Institute of Technology, February 1972; J. Ship Research, Vol.17, No.4, December 1973.

2. Tsakonas, S., Jacobs, W.R., and Ali, M.R., "Propeller Blade Pressure Distribution due to Loading and Thickness Effects," Report SIT-DL-76-1869, Stevens Institute of Technology, April 1976; J. Ship Research, Vol.23, No.2, June 1979.

3. Jacobs, W.R. and Tsakonas, S., "Generalized Lift Operator Technique for the Solution of the Downwash Integral Equation," Davidson Laboratory Report 1308, Stevens Institute of Technology, August 1968; published as "A New Procedure for the Solution of Lifting Surface Problems," J. Hydronautics, Vol.3, No.1, January 1969.

4. Tsakonas, S. and Jacobs, W.R., "Propeller Loading Distributions," Davidson Laboratory Report 1319, Stevens Institute of Technology, August 1968; J. Ship Research, Vol.13, No.4, December 1969.

5. Van Dyke, M.D., "Second-Order Subsonic Airfoil Theory Including Edge Effects," NACA Report 1274, 1956.

6. Lighthill, M.J., "A New Approach to Thin Aerofoil Theory," Aero. Quart., Vol.3, Pt.3, November 1951.

7. Goodman, T.R., "Note on the Velocity Field Induced by a Propeller Inside Its Race by Means of Lifting Surface Theory," Davidson Laboratory Technical Note (unpublished).

8. Kerwin, J.E. and Leopold, R., "Propeller Incidence Correction Due to Blade Thickness," J. Ship Research, Vol.7, No.2, October 1963.

9. Hoerner, S.F., Fluid-Dynamic Drag, published by the author, 1965.

10. Miller, M.L., "Experimental Determination of Unsteady Propeller Forces," Proceedings, Seventh ONR Symposium on Naval Hydrodynamics, Office of Naval Research, August 1968, pp.225-290.

11. Denny, S.B., "Cavitation and Open Water Performance Tests of a Series of Propellers Designed by Lifting Surface Methods," NSRDC Rept 2878, Naval Ship Research and Development Center, September 1968.

12. Kerwin, J.E. and Chang-Sup Lee, "Prediction of Steady and Unsteady Marine Propeller Performance by Numerical Lifting-Surface Theory," Presented at the Annual Meeting of SNAME, New York, November 1978.

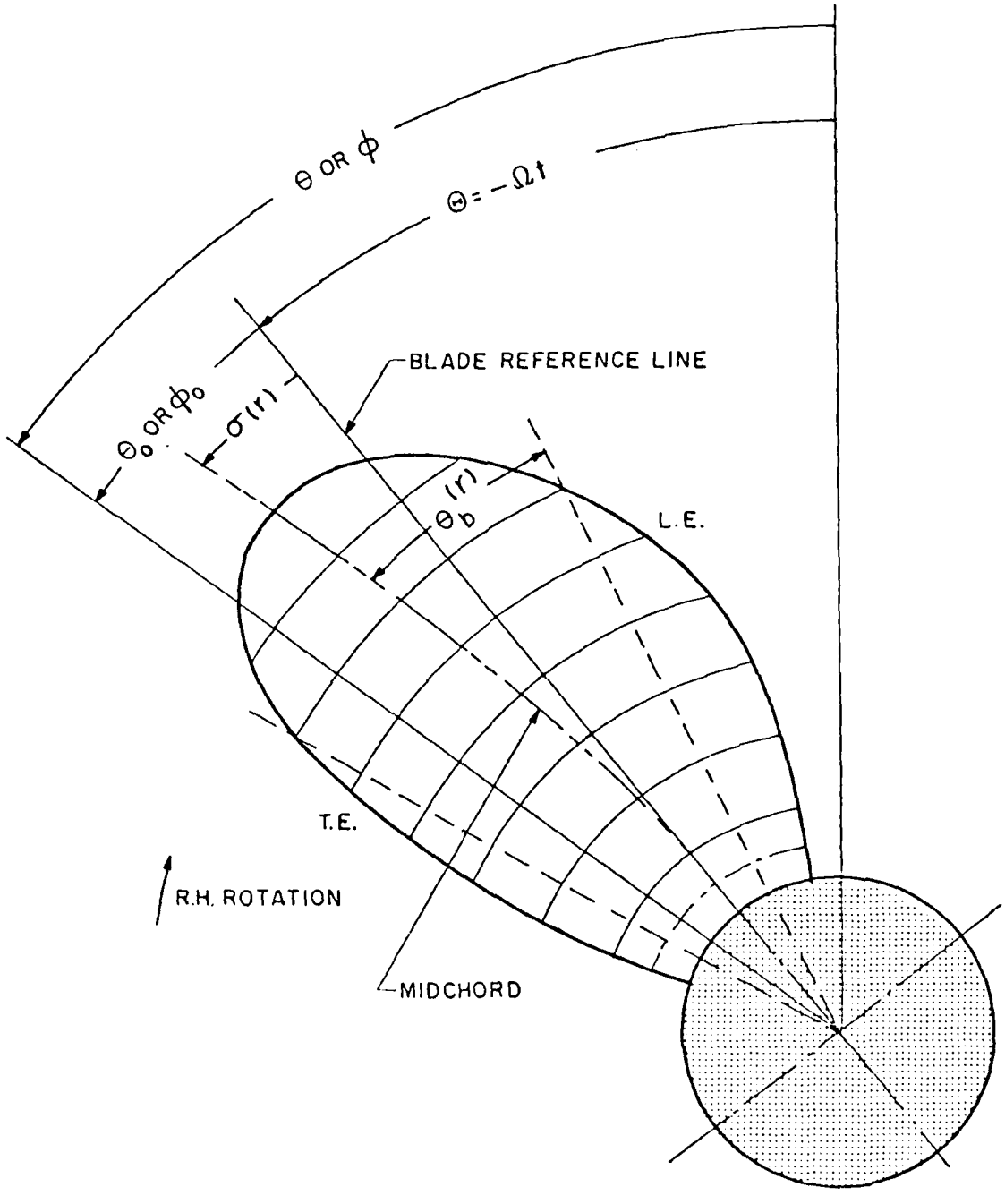

FIGURE 1. DEFINITIONS OF ANGULAR MEASURES

NOTE: THE BLADE REFERENCE LINE IS THAT CONNECTING THE SHAFT CENTER WITH THE MIDPOINT OF THE CHORD AT THE HUB

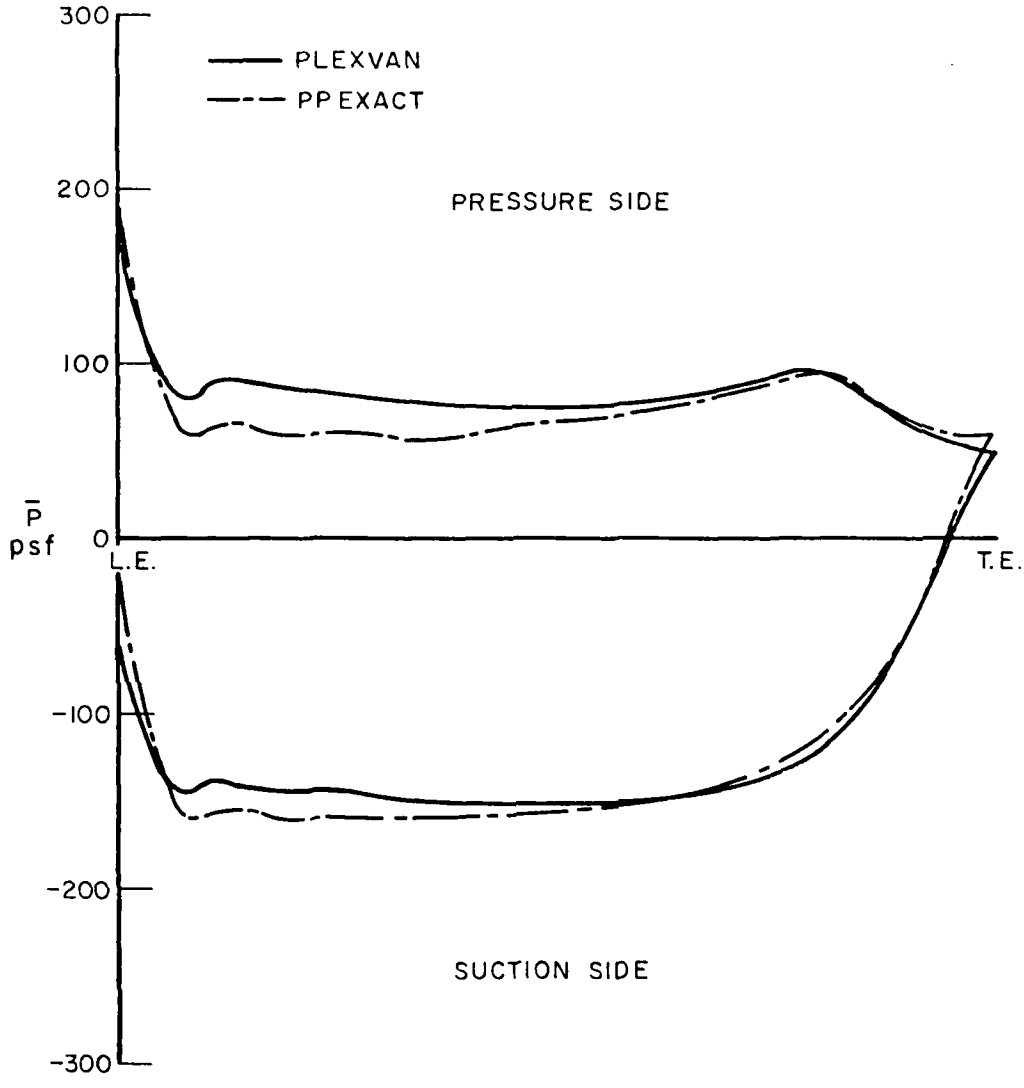

FIG. 2. STEADY-STATE CHORDWISE PRESSURE DISTRIBUTION AT 0.65 RADIUS ON DTNSRDC PROPELLER 4118 AT DESIGN J

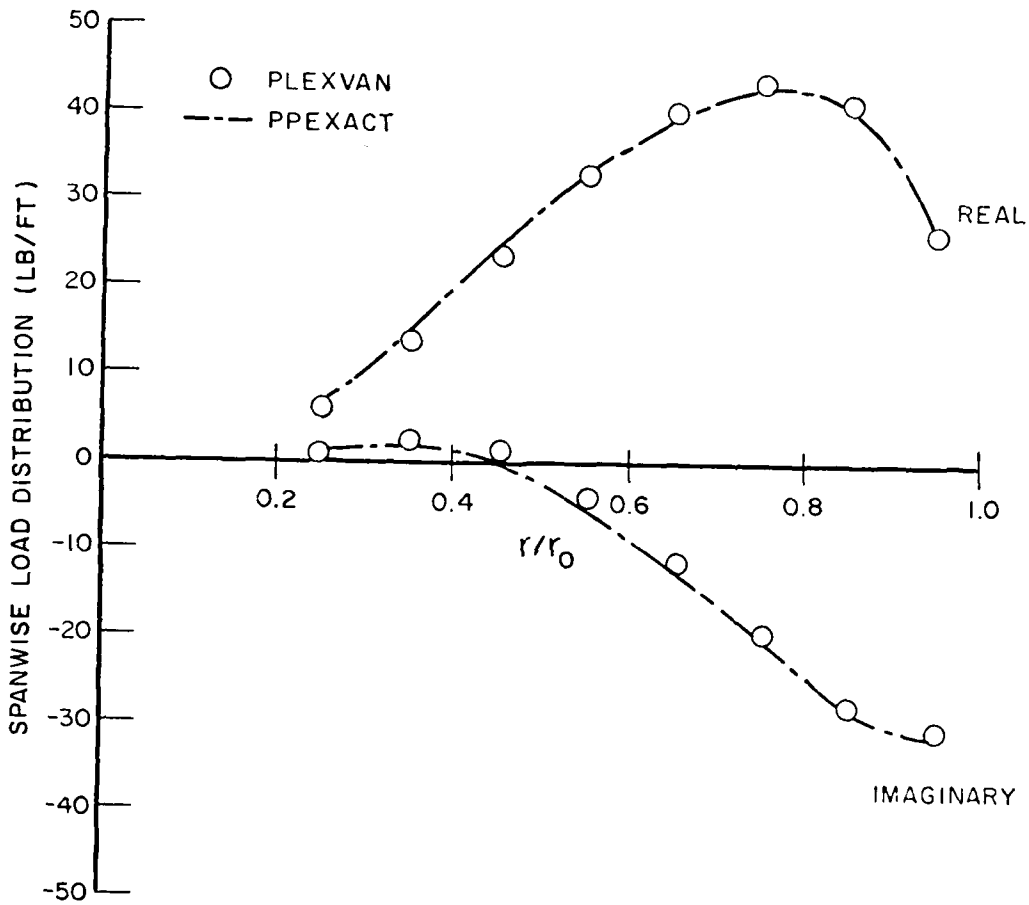

FIG. 3. BLADE FREQUENCY SPANWISE LOAD DISTRIBUTION FOR DTNSRDC PROPELLER 4118

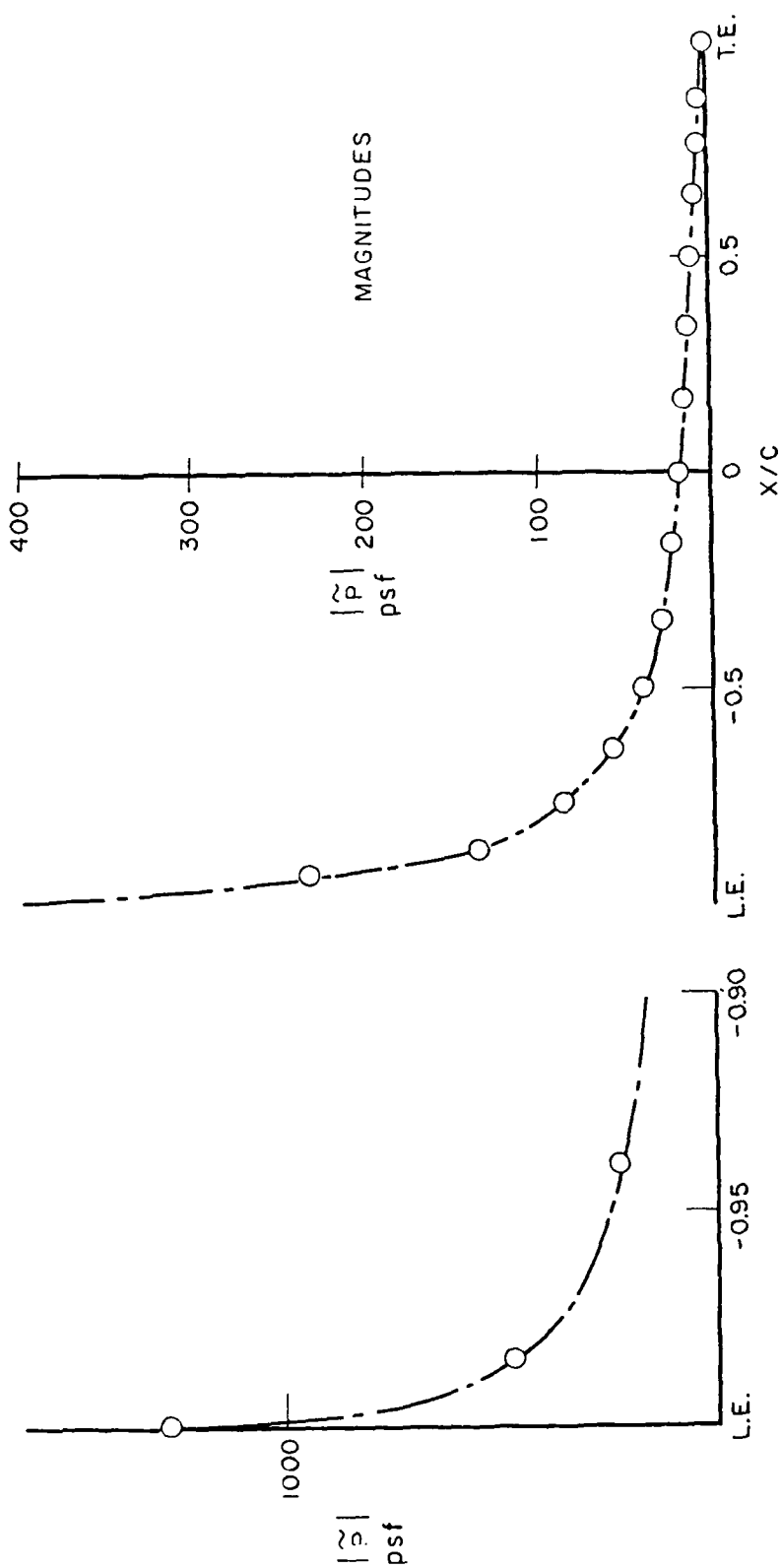

FIG.4. BLADE-FREQUENCY CHORDWISE PRESSURE DISTRIBUTION ON EACH SIDE OF DTNSRDC PROPELLER 4118 AT 0.65 RADIUS

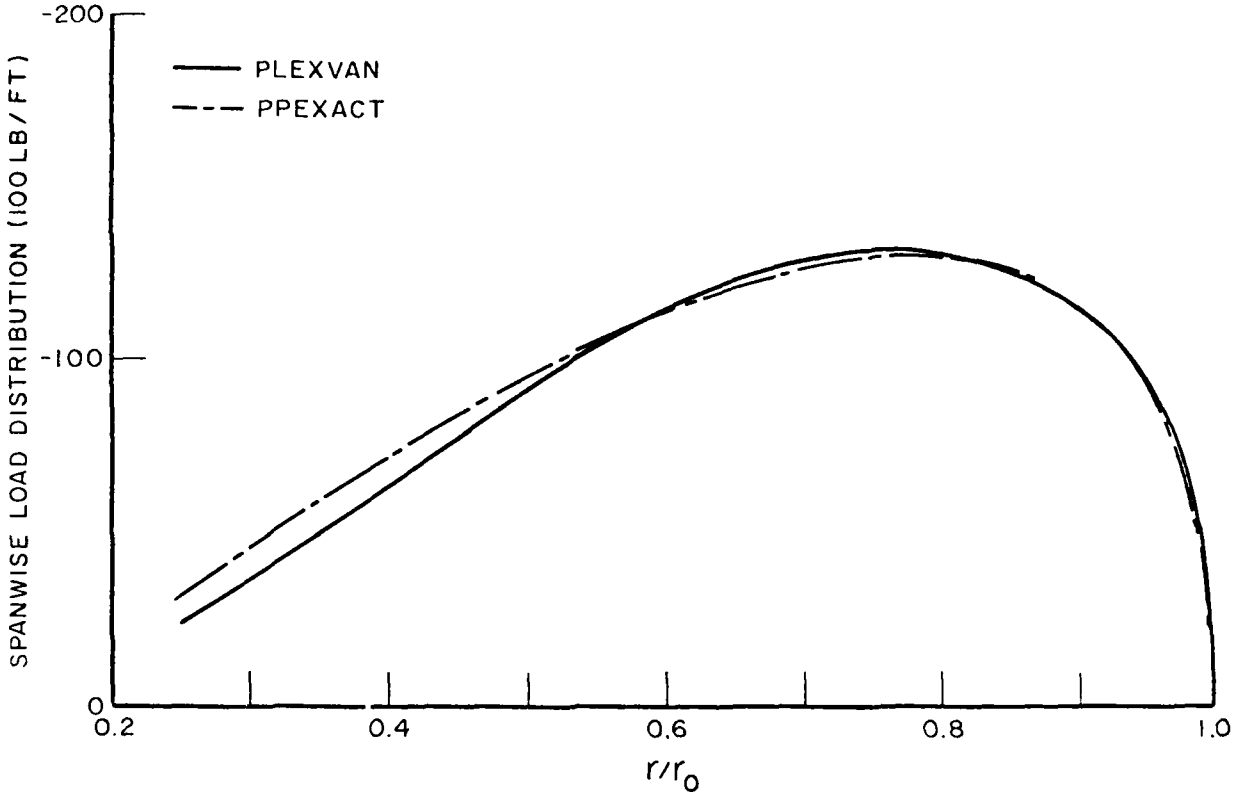

FIG. 5. STEADY STATE SPANWISE LOAD DISTRIBUTION FOR PROP. V-3275 AT J=0.993

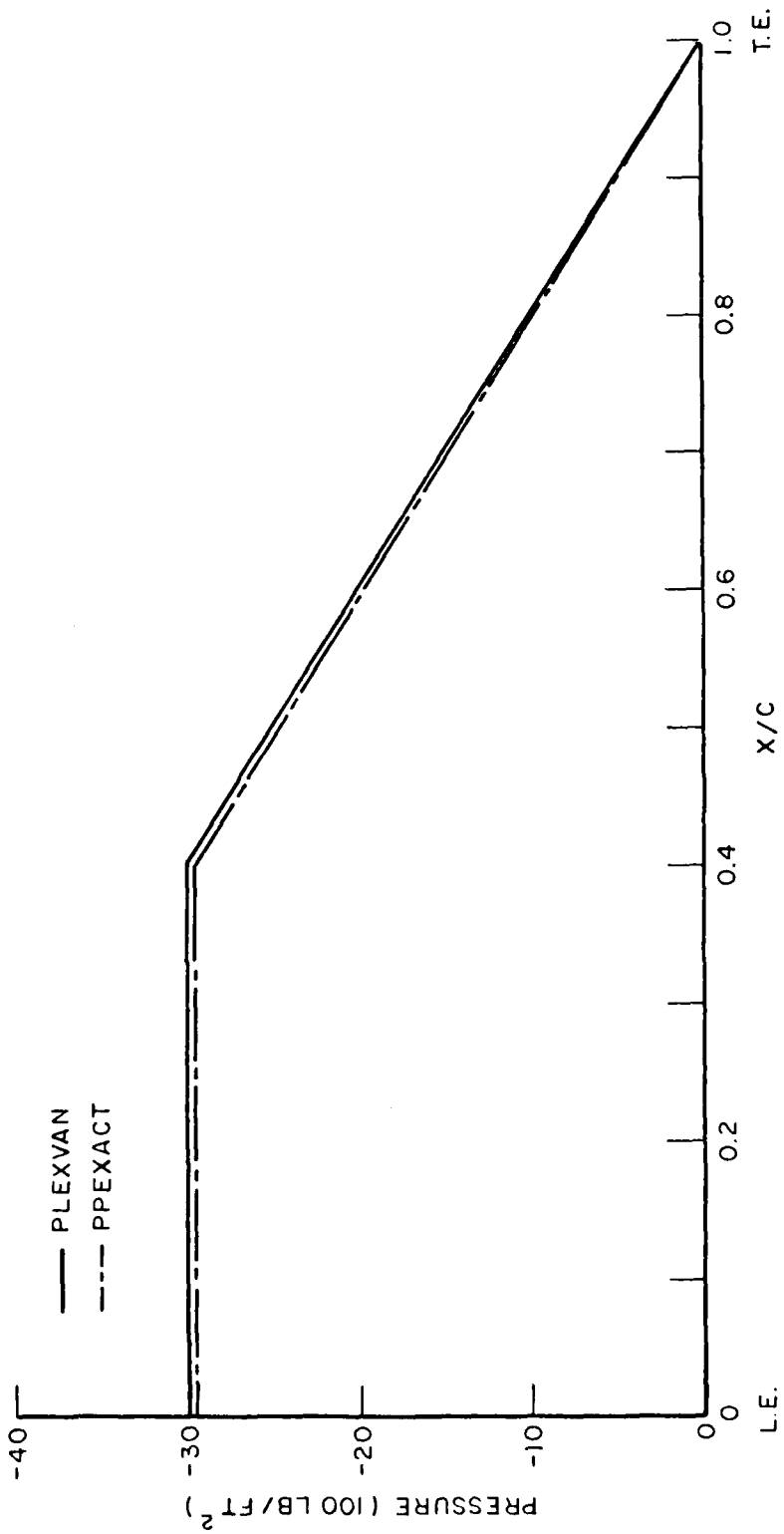

FIG.6. STEADY STATE CHORDWISE PRESSURE DISTRIBUTION FOR PROP. V-3275 AT r/r_0=0.65

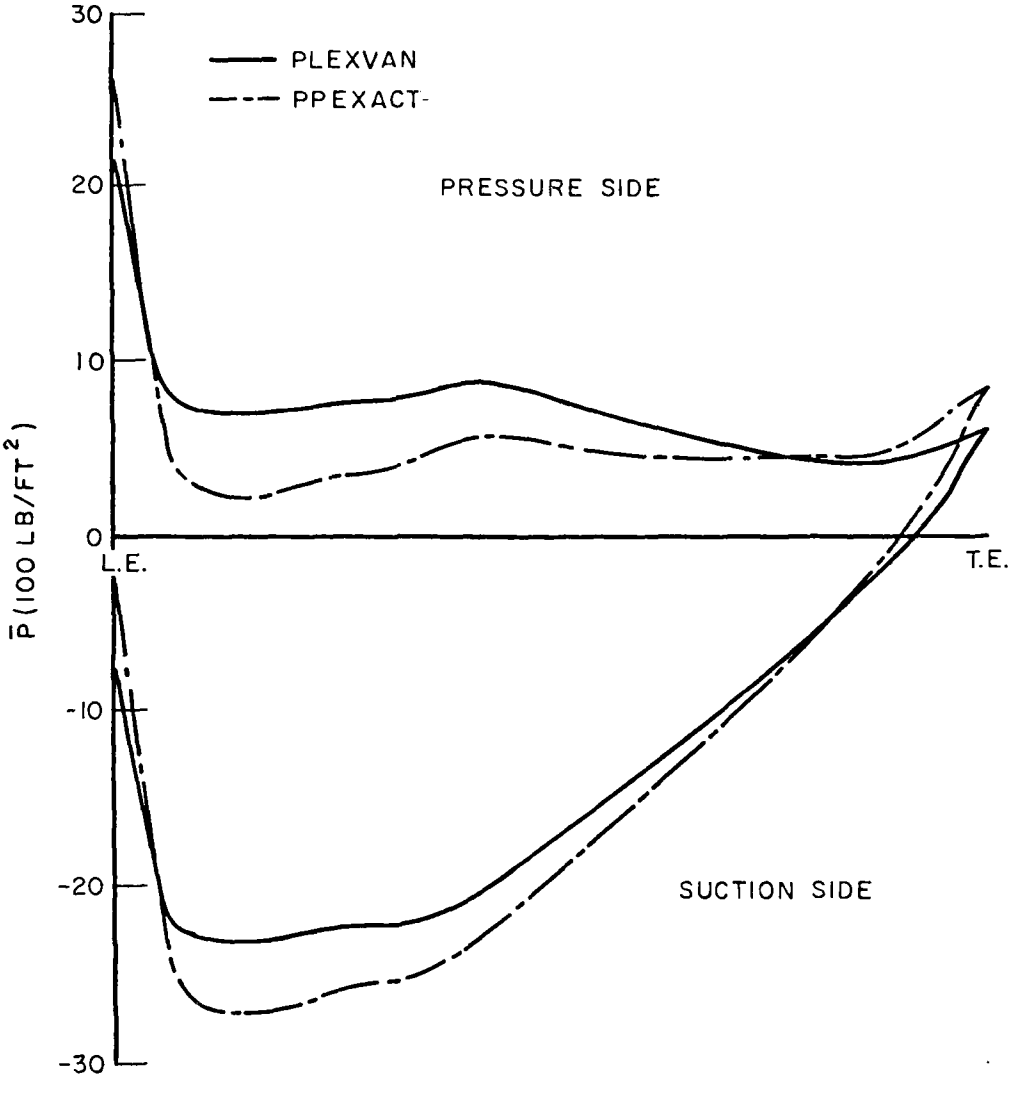

FIG. 7. STEADY STATE CHORDWISE BLADE PRESSURE DISTRIBUTION ON THE PRESSURE AND SUCTION SIDE AT r/r_0=0.65 FOR PROP. V3275

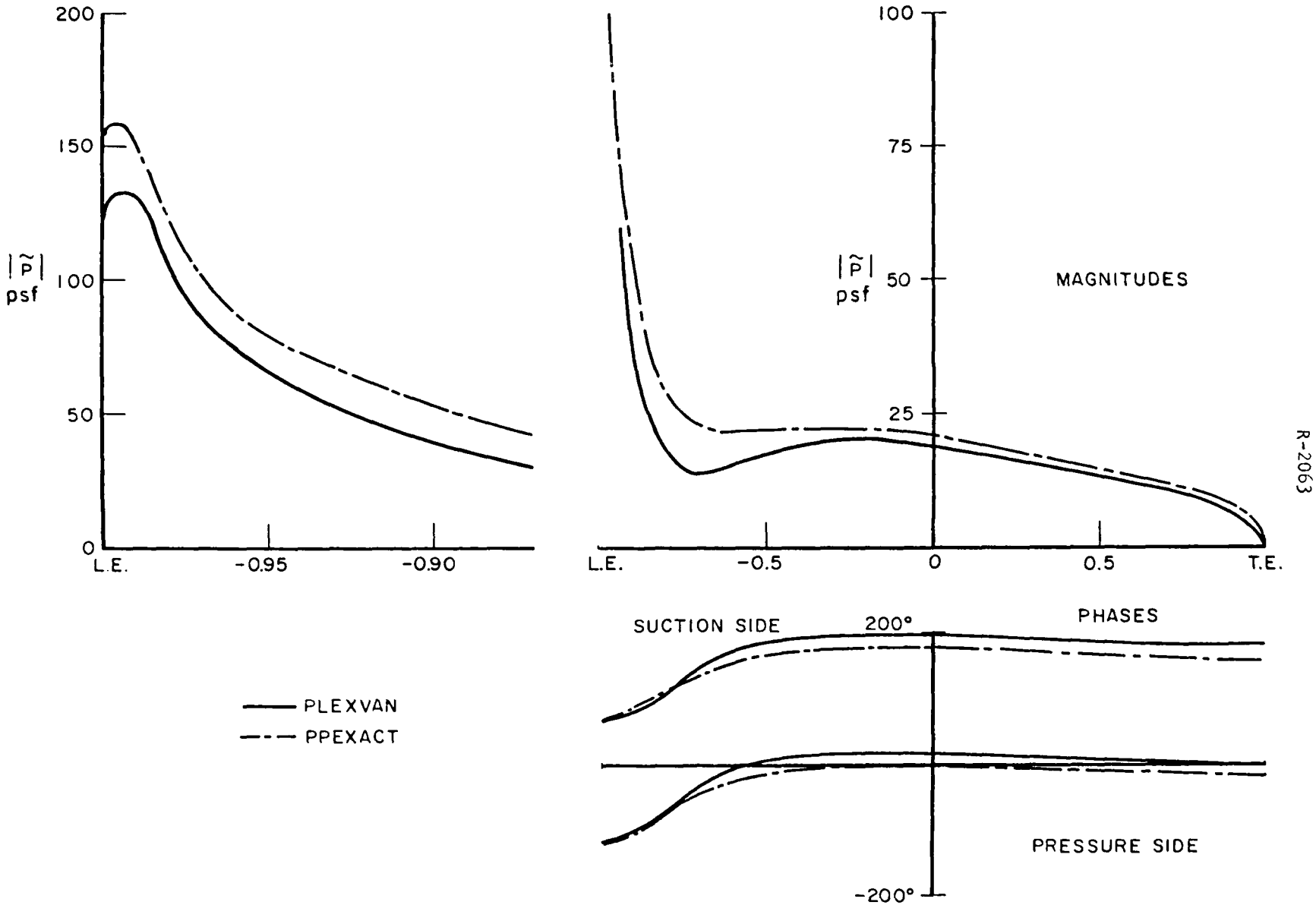

FIG. 8. BLADE FREQUENCY CHORDWISE PRESSURE DISTRIBUTION ON SUCTION AND PRESSURE SIDES FOR PROPELLER V3275 AT $r/r_0 = 0.65$

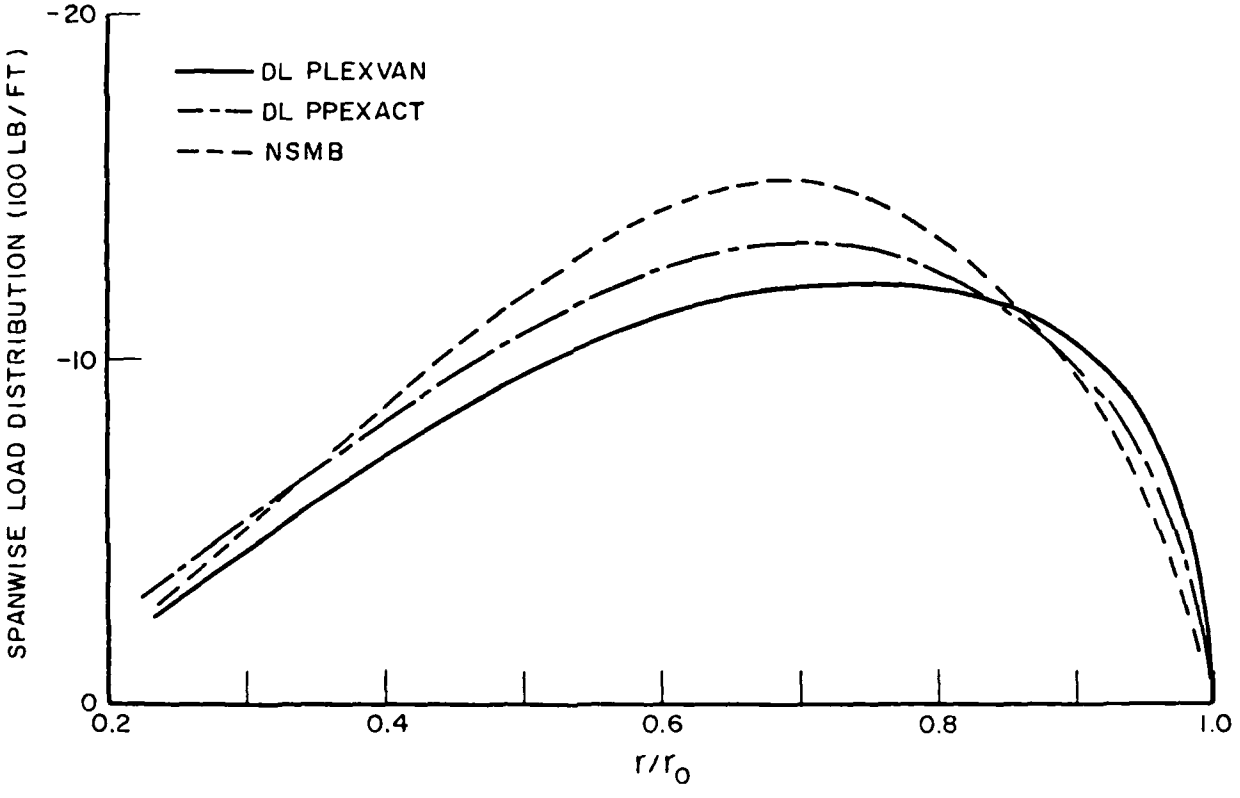

FIG. 9. STEADY STATE SPANWISE LOAD DISTRIBUTION FOR PROP. 4930, AT J=0.746

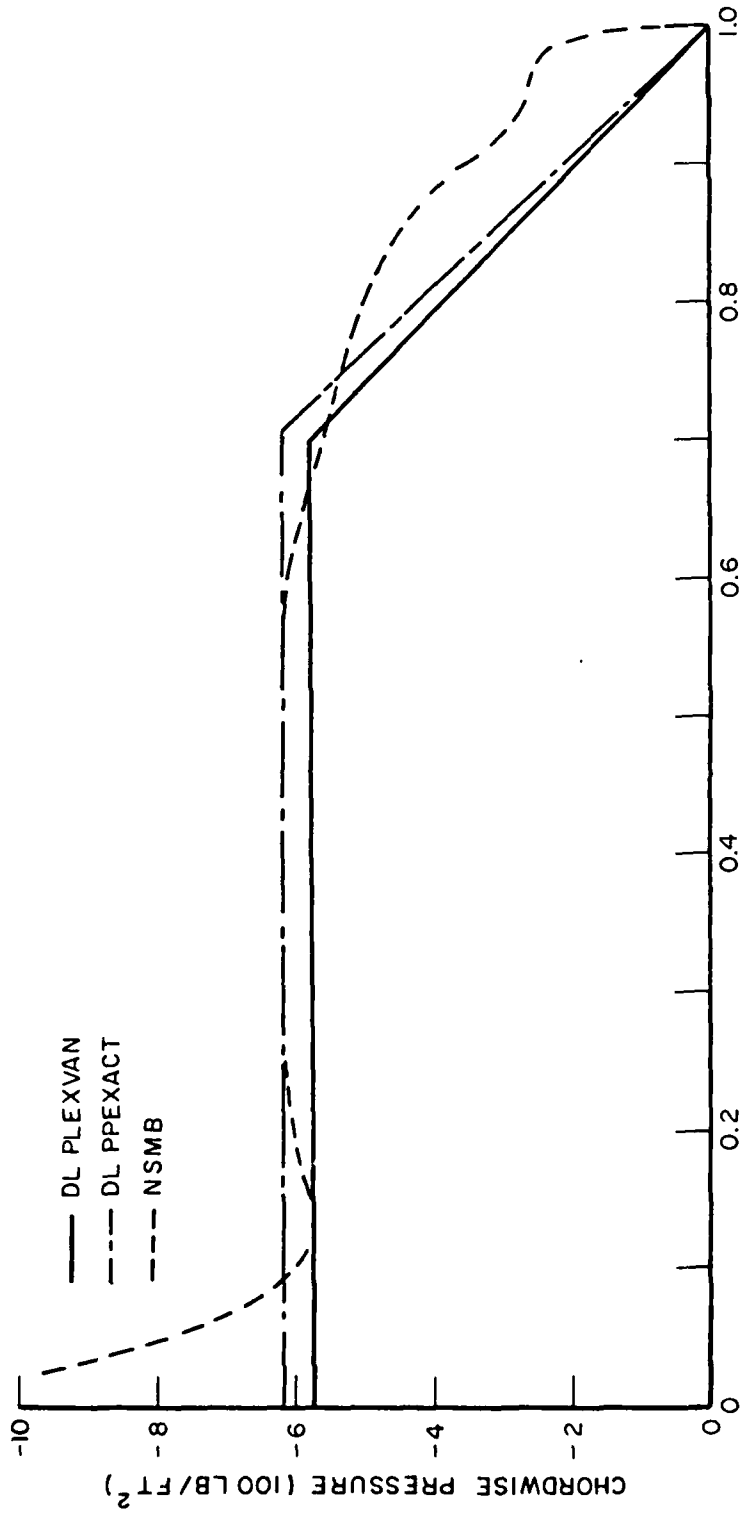

FIG. 10. STEADY STATE CHORDWISE PRESSURE DISTRIBUTION FOR PROP. 4930 AT $r/r_0 = 0.744$

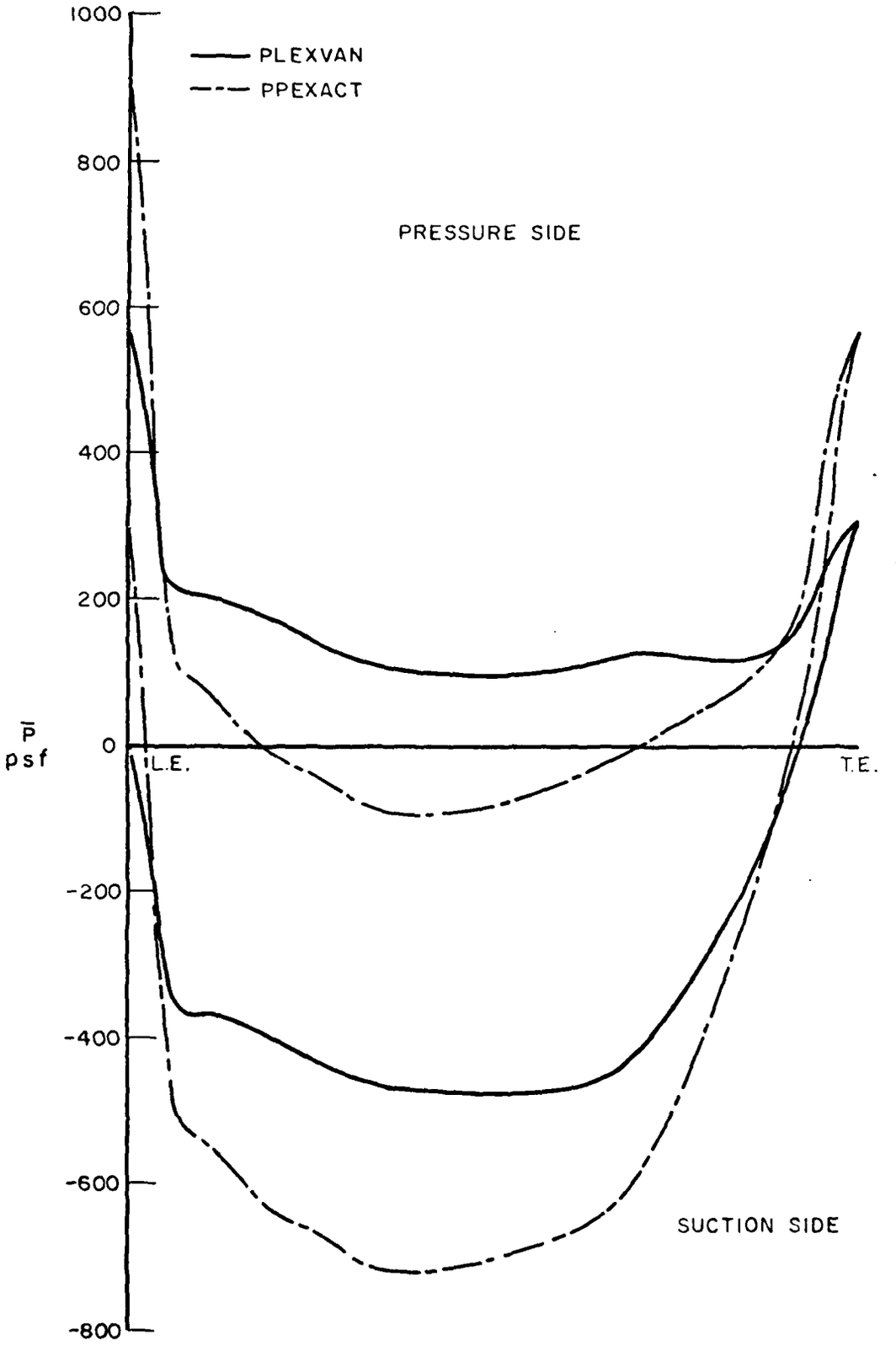

FIG.11. STEADY STATE CHORDWISE BLADE PRESSURE DISTRIBUTION ON THE PRESSURE AND SUCTION SIDES AT $r/r_0 = 0.744$ FOR PROP. 4930

APPENDIX A

Evaluation of the φ_α- and θ_α- Integrals of the Integral Equation (6)

1) $$I^{(\bar{m})}(y) = \frac{1}{\pi}\int_0^{\pi} \Phi(\bar{m}) e^{iy\cos\varphi}\, d\varphi$$

$$I^{(1)}(y) = \frac{1}{\pi}\int_0^{\pi} (1-\cos\varphi)\, e^{iy\cos\varphi}\, d\varphi = J_0(y) - iJ_1(y)$$

$$I^{(2)}(y) = \frac{1}{\pi}\int_0^{\pi} (1+2\cos\varphi)\, e^{iy\cos\varphi}\, d\varphi = J_0(y) + i2J_1(y)$$

$$I^{(\bar{m}>2)}(y) = \frac{1}{\pi}\int_0^{\pi} \cos(\bar{m}-1)\varphi\, e^{iy\cos\varphi}\, d\varphi = i^{\bar{m}-1} J_{\bar{m}-1}(y)$$

where $J_n(y)$ is the Bessel function of the first kind of order n and argument y

2) $$\Lambda^{(\bar{n})}(z) = \int_0^{\pi} \Theta(\bar{n})\, e^{-iz\cos\theta} \sin\theta\, d\theta$$

a) Birnbaum distribution

$$\Lambda^{(1)}(z) = \frac{1}{\pi}\int_0^{\pi} \cot\frac{\theta}{2}\, e^{-iz\cos\theta}\sin\theta\, d\theta = J_0(z) - iJ_1(z)$$

$$\Lambda^{(\bar{n}>1)}(z) = \frac{1}{\pi}\int_0^{\pi} \sin(\bar{n}-1)\theta\, \sin\theta\, e^{-iz\cos\theta}\, d\theta$$

$$= \frac{(-i)^{\bar{n}-2}}{2}\left[J_{\bar{n}-2}(z) + J_{\bar{n}}(z)\right]$$

b) "Roof-top" distribution ($\bar{a}$ mean lines)

$$\Lambda^{(1)}(z) = \int_0^{\cos^{-1}(1-2\bar{a})} e^{-iz\cos\theta} \sin\theta\, d\theta$$

$$+ \int_{\cos^{-1}(1-2\bar{a})}^{\pi} \frac{(1+\cos\theta)}{2(1-\bar{a})}\, e^{-iz\cos\theta} \sin\theta\, d\theta$$

$$= e^{-iz}\left\{\frac{i}{z} + \frac{1}{2(1-\bar{a})z^2}\left[e^{i2\bar{a}z} - e^{i2z}\right]\right\}$$

$$\Lambda^{(\bar{n}>1)}(z) = 0$$

(for $\bar{a}=1$, $\Lambda^{(1)}(z) = \frac{2\sin z}{z}$, and for $z=0$, $\Lambda^{(1)}(0)=1+\bar{a}$.)

Functions Required for Evaluating the Integrand of the Kernel Function at the Singularity (see Reference 2) and the Propeller-generated Moments (see text)

1) $$I_1^{(\bar{m})}(y) = \frac{1}{\pi}\int_0^{\pi} \Phi(\bar{m})\, e^{iy\cos\varphi}\cos\varphi\, d\varphi$$

$$I_1^{(1)}(y) = -\frac{1}{2}\left[J_o(y) - J_2(y)\right] + iJ_1(y)$$

$$I_1^{(2)}(y) = \left[J_o(y) - J_2(y)\right] + iJ_1(y)$$

$$I_1^{(\bar{m}>2)}(y) = \frac{i^{\bar{m}-2}}{2}\left[-J_{\bar{m}}(y) + J_{\bar{m}-2}(y)\right]$$

2) $$\Lambda_1^{\bar{m}}(z) = \int_0^{\pi} \Theta(\bar{n})\sin\theta\cos\theta\, e^{-iz\cos\theta}\, d\theta$$

a) Birnbaum distribution

$$\Lambda_1^{(1)}(z) = \frac{1}{2}\left[J_o(z) - J_2(z)\right] - iJ_1(z)$$

$$\Lambda_1^{(\bar{n}>1)}(z) = \frac{(-i)^{\bar{n}+1}}{4}\left[J_{\bar{n}-3}(z) - J_{\bar{n}+1}(z)\right]$$

b) "Roof-top distribution ($\bar{a}$ mean lines)

$$\Lambda_1^{(1)}(z) = e^{-iz}\left\{\frac{i}{z} + \frac{1}{z^2} + \frac{1}{z^2(1-\bar{a})}\left[\frac{(1-2\bar{a}}{2} - \frac{i}{z}\right) e^{i2\bar{a}z} + \left(\frac{1}{2} + \frac{i}{z}\right) e^{i2z}\right]\right\}$$

(For $\bar{a} = 1$, $\Lambda_1^{(1)}(z) = \frac{i2}{z}\left(\cos z - \frac{\sin z}{z}\right)$.)

It is to be noted that the values for negative argument, i.e., $I^{(\bar{m})}(-y)$, $I_1^{(\bar{m})}(-y)$, $\Lambda^{(\bar{n})}(-z)$ and $\Lambda_1^{(\bar{n})}(-z)$, are the conjugates of the values given above.

APPENDIX B

Normal Velocity Due to "Nonplanar" Blade Thickness

The following substitutions are made in Equations (15) and (16) of the text

$$d\theta_o = \theta_b^\rho \sin\theta_\alpha d\theta_\alpha$$

$$\frac{\partial f_\tau(\xi,\rho,\theta_o)}{\partial\xi} = \frac{a_A(\rho)}{\theta_b^\rho \sin\theta_\alpha} \frac{\partial f_\tau(\rho,\theta_\alpha)}{\partial\theta_\alpha}$$

$$\frac{1}{R} = \frac{1}{\pi} \sum_{m=-\infty}^{\infty} e^{im(\theta_o-\varphi_o+\bar{\theta}_n)} \int_{-\infty}^{\infty} (IK)_m \, e^{iu(x-\xi)} du$$

where

$$(IK)_m = \begin{cases} I_m(|u|\rho)K_m(|u|r) & \text{for } \rho < r \\ I_m(|u|r)K_m(|u|\rho) & \text{for } r < \rho \end{cases}$$

$$\frac{\partial}{\partial n'} = \frac{r}{\sqrt{1+a_A^2(r)\,r^2}} \left(a_A(r) \frac{\partial}{\partial x} - \frac{1}{r^2} \frac{\partial}{\partial\varphi_o} \right)$$

Since $\sum_{n=1}^{N} e^{im\bar{\theta}_n} = \begin{cases} N & \text{for } m=\ell N, \quad \ell = 0,\pm1,\pm2,\ldots \\ 0 & \text{otherwise} \end{cases}$, Equation (16) becomes

$$\frac{V_\tau^{(o)}(r)}{U_A(r)} = \frac{iNr}{2\pi^2 U_A(r)\sqrt{1+a_A^2(r)\,r^2}} \sum_{\substack{m=-\infty \\ m=\ell N}} \int_0^\pi \int_0^\infty U_A(\rho)\sqrt{1+a_A^2(\rho)\,\rho^2} \frac{\partial f_\tau}{\partial\theta_\alpha} e^{im(\theta_o-\varphi_o)}$$

$$\cdot \int_{-\infty}^{\infty} \left(a_A(r)u + \frac{m}{r^2} \right) (IK)_m e^{i(x-\xi)u} du\, d\rho\, d\theta_\alpha \qquad \text{(B-1)}$$

With the trigonometric transformations for x, φ_o, ξ, and θ_o given in the text, the series is brought to

$$\sum_{\substack{m=-\infty \\ m=\ell N}}^{\infty} \int_0^{\pi} \int_{\rho} U_A(\rho)\sqrt{1+a_A^2(\rho)\rho^2}\ \frac{\partial f_\tau}{\partial\theta_\alpha}\ e^{-im(\sigma^r-\sigma^\rho)}$$

$$\cdot \int_{-\infty}^{\infty} \left(a_A(r)u + \frac{m}{r^2}\right)(IK)_m\, e^{iu(\sigma^r/a_A(r)-\sigma^\rho/a_A(\rho))}\ e^{i(u-a_A(\rho)m)\theta_b^\rho\cos\theta_\alpha/a_A(\rho)}$$

$$\cdot\ e^{-i(u-a_A(r)m)\theta_b^r\cos\varphi_\alpha/a_A(r)}\ du d\rho d\theta_\alpha \qquad \text{(B-2)}$$

Let

$$A((u-a_A(\rho)m)\theta_b^\rho/a_A(\rho)) = \int_0^{\pi} \frac{\partial f_\tau}{\partial\theta_\alpha}\, e^{i((u-a_A(\rho)m)\theta_b^\rho/a_A(\rho))\cos\theta_\alpha} d\theta_\alpha$$

and applying the generalized lift operator (see Appendix A)

$$\frac{V_\tau^{(o)}(r)}{U_A(r)} = \frac{iNr}{2\pi^2 U_A(r)\sqrt{1+a_A^2(r)r^2}} \int_{\rho} U_A(\rho)\sqrt{1+a_A^2(\rho)\rho^2}$$

$$\cdot \sum_{\ell=-\infty}^{\infty} e^{-i\ell N(\sigma^r-\sigma^\rho)} \int_{-\infty}^{\infty} \left(a_A(r)u + \frac{\ell N}{r^2}\right)(IK)_{\ell N} e^{iu(\sigma^r/a_A(r)-\sigma^\rho/a_A(\rho))}$$

$$\cdot A\left((u-a_A(\rho)\ell N)\theta_b^\rho/a_A(\rho)\right) I^{(\bar{m})}\left((a_A(r)\ell N-u)\theta_b^r/a_A(r)\right) du d\rho \qquad \text{(B-3)}$$

It can readily be seen that folding the doubly infinite ℓ-series and u-integration yields Equation (17) of the text.

APPENDIX C

Thickness Effects (Non-lifting)

The velocity potential due to source-sink distributions approximating the symmetrical thickness distribution of an N-bladed propeller is given by

$$\Phi(x,r,\varphi_o;0) = -\frac{1}{4\pi}\sum_{n=1}^{N}\iint_S \frac{M(\rho,s)}{R}\,dS$$

$$= -\frac{1}{4\pi}\sum_{n=1}^{N}\int_0^{\pi}\int_{\rho}^{\rho_b}\frac{M(\rho,s)}{R}\,\frac{\sqrt{1+a^2(\rho)\rho^2}}{a(\rho)\rho}\,\rho\,\sin\theta_\alpha\,d\theta_\alpha\,d\rho \qquad (C-1)$$

where the source strength is

$$M(\rho,s) = 2U_A(\rho)\sqrt{1+a^2(\rho)\rho^2}\,\frac{\partial f_T(\rho,s)}{ds} = 2U_A(\rho)\,\frac{\partial f_T(\xi,\rho,\theta_o)}{\partial\xi}$$

the Descartes distance R is

$$\left[(x-\xi)^2 + r^2 + \rho^2 - 2r\rho\,\cos\left(\theta_o-\varphi_o+\bar{\theta}_n\right)\right]^{\frac{1}{2}}$$

s is measured along the chord of the blade section and the other symbols are as defined in the text.

From Bernoulli's equation, the linearized pressure P_T is

$$P_T(x,r,\varphi_o) = -\rho_f U_A(r)\left(\frac{\partial\Phi}{\partial x} + a(r)\,\frac{\partial\Phi}{\partial\varphi_o}\right)$$

Hence

$$P_T(x,r,\varphi_o) = \frac{\rho_f U_A(r)}{2\pi}\sum_{n=1}^{N}\int_0^{\pi}\int_{\rho}^{\rho_b} U_A(\rho)\,\frac{\partial f_T(\xi,\rho,\theta_o)}{a(\rho)\partial\xi}\left[\left(\frac{\partial}{\partial x}+a(r)\frac{\partial}{\partial\varphi_o}\right)\frac{1}{R}\right]\rho\,\sqrt{1+a^2(\rho)\rho^2}\,\sin\theta_\alpha\,d\theta_\alpha\,d\rho \qquad (C-2)$$

If use is made of the expansion

$$\frac{1}{R} \equiv \frac{1}{\pi}\sum_{m=-\infty}^{\infty} e^{im(\theta_o-\varphi_o+\bar{\theta}_n)}\int_{-\infty}^{\infty}(IK)_m\,e^{i(x-\xi)k}\,dk$$

where

$$(IK)_m = \begin{cases} I_m(|k|\rho)K_m(|k|r) & \text{for } \rho < r \\ I_m(|k|r)K_m(|k|\rho) & \text{for } r < \rho \end{cases}$$

then

$$\left(\frac{\partial}{\partial x} + a(r)\,\frac{\partial}{\partial \varphi_o}\right)\frac{1}{R} = \frac{i}{\pi}\sum_{m=-\infty}^{\infty} e^{im(\theta_o - \varphi + \bar{\theta}_o)} \int_{-\infty}^{\infty} (k - a(r)m)\,(IK)_m\, e^{i(x-\xi)k}\,dk \tag{C-3}$$

Since

$$\xi = \theta_o/a(\rho) = (\sigma^\rho - \theta_b^\rho \cos\theta_\alpha)/a(\rho)$$

$$\frac{\partial f_\tau(\xi,\rho,\theta_o)}{\partial \xi} = -\frac{a(\rho)}{\theta_b^\rho \sin\theta_\alpha}\,\frac{\partial f_\tau(\rho,\theta_\alpha)}{\partial \theta_o} \tag{C-4}$$

Also

$$\sum_{n=1}^{N} e^{im\bar{\theta}_n} = \begin{cases} N \text{ for } m = \ell N\,,\ \ell = 0, \pm 1, \pm 2, \ldots \\ 0 \text{ for } m \neq \ell N \end{cases} \tag{C-5}$$

On substituting Eqs.(C-3) - (C-5) in Eq.(B-2), the pressure becomes

$$P_\tau(x,r,\varphi_o) = \frac{iN\rho_f U_A(r)}{2\pi^2} \int_0^\pi \int_\rho \frac{\partial f_\tau(\rho,\theta_\alpha)}{\partial \theta_\alpha}\,\sqrt{1 + a^2(\rho)\rho^2}\cdot U_A(\rho)$$

$$\cdot \sum_{\substack{m=-\infty \\ m=\ell N}}^{\infty} e^{im(\theta_o - \varphi_o)} \int_{-\infty}^{\infty} (k - a(r)m)\,(IK)_m\, e^{i(x-\xi)k}\,dk\,d\theta_\alpha\,d\rho \tag{C-6}$$

With the trigonometric transformations for θ_o and φ_o

$$P_\tau(x,r,\varphi_o) = \frac{iN\rho_f U_A(r)}{2\pi^2} \sum_{\substack{m=-\infty \\ m=\ell N}}^{\infty} \int_0^\pi \int_\rho \frac{\partial f_\tau(\rho,\theta_\alpha)}{\partial \theta_\alpha}\sqrt{1 + a^2(\rho)\rho^2}\; U_A(\rho)\, e^{-im\Delta\sigma}\, e^{im(\theta_b^r \cos\varphi_\alpha - \theta_b^\rho \cos\theta_\alpha)}$$

$$\cdot \int_{-\infty}^{\infty} \left(k - a(r)m\right)(IK)_m\, e^{ik\left(\frac{\sigma^r}{a(r)} - \frac{\sigma^\rho}{a(\rho)}\right)}\, e^{-ik\left(\frac{\theta_b^r}{a(r)}\cos\varphi_\alpha - \frac{\theta_b^\rho}{a(\rho)}\cos\theta_\alpha\right)} dk\,d\theta_\alpha\,d\rho \tag{C-7}$$

The θ_α-integral is as before (see Eq.17 of text)

$$A\left(\left(k-a(\rho)m\right)\theta_b^\rho/a(\rho)\right) = \int_0^\pi \frac{\partial f_T(\rho,\vartheta_\alpha)}{\partial\theta_\alpha}\, e^{i\left((k-a(\rho)m)\theta_b^\rho/a(\rho)\right)\cos\theta_\alpha}\, d\theta_\alpha \qquad (C\text{-}8)$$

After folding the m-series to $m=0$ to $+\infty$, the pressure of Eq.(C-7) is brought to

$$P_T(x,r,\varphi_o) = \frac{iN\rho_f U_A(r)}{2\pi^2} \int_\rho \sqrt{1+a^2(\rho)\rho^2}\cdot U_A(\rho)$$

$$\cdot \left\{ \int_{-\infty}^{\infty} A\left(k\theta_b^\rho/a(\rho)\right) k(IK)_o e^{ik\left(\frac{\sigma^r}{a(r)} - \frac{\sigma^\rho}{a(\rho)} - \frac{\theta_b^r}{a(r)}\cos\varphi_\alpha\right)} dk \right.$$

$$+ \sum_{m=N,2N}^{M} \int_{-\infty}^{\infty} (IK)_m \left[A\left((k-a(\rho)m)\theta_b^\rho/a(\rho)\right)\left(k-a(r)m\right) e^{i(k-a(r)m)(\sigma^r-\theta_b^r\cos\varphi_\alpha)/a(r)}\, e^{-i(k-a(\rho)m)\sigma^\rho/a(\rho)} \right.$$

$$\left. \left. + A\left((k+a(\rho)m)\theta_b^\rho/a(\rho)\right)\left(k+a(r)m\right) e^{i(k+a(r)m)(\sigma^r-\theta_b^r\cos\varphi_\alpha)/a(r)}\, e^{-i(k+a(\rho)m)\sigma^\rho/a(\rho)} \right] dk \right\} d\rho$$

(C-9)

Let $k-a(\rho)m=u$ in the first term and $k+a(\rho)m=u$ in the second term of the second k-integral. Finally, Eq.(C-9) can be written (for $\rho < r$) as

$$P_T(x,r,\varphi_o) = -\frac{N\rho_f U_A(r)}{\pi^2} \int_\rho U_A(\rho)\sqrt{1+a^2(\rho)\rho^2}$$

$$\cdot \left\{ \int_0^\infty u I_o(u\rho) K_o(ur) \left\{ \mathrm{ImPart}\left[A\left(u\theta_b^\rho/a(\rho)\right) e^{iu(\sigma^r-\theta_b^r\cos\varphi)/a(r)}\, e^{-iu\sigma^\rho/a(\rho)} \right] \right\} du \right.$$

$$+ \sum_{m=N,2N}^{M} \int_0^\infty \left[u-\left(a(r)-a(\rho)\right)m \right] I_m(|u+a(\rho)m|\rho) K_m(|u+a(\rho)m|r)$$

$$\left. \cdot \left\{ \mathrm{ImPart}\left[A\left(u\theta_b^\rho/a(\rho)\right) e^{i\left[u-(a(r)-a(\rho))m\right](\sigma^r-\theta_b^r\cos\varphi_\alpha)/a(r)}\, e^{-iu\sigma^\rho/a(\rho)} \right] \right\} du \right.$$

(C-10)

[Cont'd]

$$+ \sum_{m=N,2N}^{M} \int_{o}^{\infty} \left[u+\left(a(r)-a(\rho)\right)\right] I_m(|u-a(\rho)m|\rho) K_m(|u-a(\rho)m|r)$$

$$\cdot \left\{ \text{ImPart}\left[A\left(u\theta_b^{\rho}/a(\rho)\right) e^{i[u+(a(r)-a(\rho))m](\sigma^r-\theta_b^r\cos\varphi_\alpha)/a(r)} e^{-iu\sigma^{\rho}/a(\rho)} \right] \right\} du \qquad \text{(C-10)}$$

DISTRIBUTION LIST

(Contract N00014-77-C-0059)

25 Commander
DAVID W. TAYLOR NAVAL SHIP
R&D CENTER (Attn: Code 1505)
Bethesda, MD 20084

Officer-in-Charge
Annapolis Laboratory
DAVID W. TAYLOR NAVAL SHIP
R&D CENTER (Code 522.3)
Annapolis, MD 21402

9 Commander
NAVAL SEA SYSTEMS COMMAND
Washington, DC 20362
Attn: SEA 32R
312
3213
05H
05R11
52
521
524
99612

12 Director
DEFENSE TECHNICAL INFORMATION
CENTER
5010 Duke Street
Alexandria, VA 22314

OFFICE OF NAVAL RESEARCH
800 N. Quincy Street
Arlington, VA 22217
Attn: Code 438

OFFICE OF NAVAL RESEARCH
BRANCH OFFICE (493)
536 S. Clark Street
Chicago, IL 60605

Chief Scientist
OFFICE OF NAVAL RESEARCH WESTERN
REGIONAL OFFICE
1030 E. Green Street
Pasadena, CA 91106

OFFICE OF NAVAL RESEARCH
Resident Representative
715 Broadway (5th Floor)
New York, NY 10003

OFFICE OF NAVAL RESEARCH
San Francisco Area Office
760 Market Street, Room 447
San Francisco, CA 94102

Director (Code 2027)
NAVAL RESEARCH LABORATORY
Washington, DC 20390

LIBRARY OF CONGRESS
Science & Technology Division
Washington, DC 20540

Mr. D. Blount (6661)
NAVAL SEA SYSTEMS COMMAND
DETACHMENT
Naval Station
Norfolk, VA 23511

NAVAL UNDERWATER WEAPONS RESEARCH
& ENGINEERING STATION (Library)
Newport, RI 02840

Commanding Office (L31)
NAVAL CIVIL ENGINEERING LABORATORY
Port Hueneme, CA 93043

4 Commander
NAVAL OCEAN SYSTEMS CENTER
San Diego, CA 92152
Attn: Dr. A. Fabula (4007)
Dr. J. Hoyt (2501)
Dr. M. Reichman (6342)
Library

Library
NAVAL UNDERWATER SYSTEMS CENTER
Newport, RI 02840

Research Center Library
WATERWAYS EXPERIMENT STATION
CORPS OF ENGINEERS
P.O. Box 631
Vicksburg, MS 39180

CHARLESTON NAVAL SHIPYARD
Technical Library
Naval Base
Charleston, SC 29408

DISTRIBUTION LIST

(Contract N00014-77-C-0059)

NORFOLK NAVAL SHIPYARD
Technical Library
Portsmouth, VA 23709

PORTSMOUTH NAVAL SHIPYARD
Technical Library
Portsmouth, NH 03801

PUGET SOUND NAVAL SHIPYARD
Engineering Library
Bremerton, WA 98314

LONG BEACH NAVAL SHIPYARD
Technical Library (246L)
Long Beach, CA 90801

MARE ISLAND NAVAL SHIPYARD
Shipyard Technical Library (202.3)
Vallejo, CA 94592

Assistant Chief Design Engineer for
Naval Architecture (Code 250)
MARE ISLAND NAVAL SHIPYARD
Vallejo, CA 94592

2 U.S. NAVAL ACADEMY
Annapolis, MD 21402
Attn: Technical Library
Dr. S.A. Elder

NAVAL POSTGRADUATE SCHOOL
Monterey, CA 93940
Attn: Library (2124)

Study Center
National Maritime Research Center
U.S. MERCHANT MARINE ACADEMY
Kings Point
Long Island, NY 11024

THE PENNSYLVANIA STATE UNIVERSITY
Applied Research Laboratory (Library)
P.O. Box 30
State College, PA 16801

Library
BOLT, BERANEK & NEWMAN
50 Moulton Street
Cambridge, MA 02138

BETHLEHEM STEEL CORPORATION
25 Broadway
New York, NY 10004
Attn: Library - Shipbuilding

R&D Manager
Electric Boat Division
GENERAL DYNAMICS CORPORATION
Groton, CT 06340

GIBBS & COX, INC.
Technical Information Control
21 West Street
New York, NY 10006

Library
HYDRONAUTICS, INC.
Pindell School Road
Laurel, MD 20810

2 MCDONNELL DOUGLAS AIRCRAFT COMPANY
3855 Lakewood Blvd
Long Beach, CA 90801
Attn: Dr. T. Cebeci
Mr. J. Hess

NEWPORT NEWS SHIPBUILDING AND
DRY DOCK COMPANY (TECH LIBRARY)
4101 Washington Avenue
Newport News, VA 23607

Mr. S. Spangler
NIELSEN ENGINEERING & RESEARCH, INC.
510 Clyde Avenue
Mountain View, CA 94043

SOCIETY OF NAVAL ARCHITECTS AND
MARINE ENGINEERS
Technical Library
One World Trade Center, Suite 1369
New York, NY 10048

SUN SHIPBUILDING & DRY DOCK CO.
Attn: Chief Naval Architect
Chester, PA 19000

Library
SPERRY SYSTEMS MANAGEMENT DIV.
SPERRY RAND CORPORATION
Great Neck, NY 11020

DISTRIBUTION LIST
(Contract N00014-77-C-0059)

Dr. B. Parkin, Director
Garfield Thomas Water Tunnel
APPLIED RESEARCH LABORATORY
P.O. Box 30
State College, PA 16801

STANFORD RESEARCH INSTITUTE
Library
Menlo Park, CA 94025

2 SOUTHWEST RESEARCH INSTITUTE
P.O. Drawer 28510
San Antonio, TX 78284
Attn: Applied Mechanics Review
Dr. H. Abramson

TRACOR, INC.
6500 Tracor Lane
Austin, TX 78721

Mr. Robert Taggart
9411 Lee Highway, Suite P
Fairfax, VA 22031

Ocean Engineering Department
WOODS HOLE OCEANOGRAPHIC, INC.
Woods Hole, MA 02543

Technical Library
Alden Research Laboratory
WORCESTER POLYTECHNIC INSTITUTE
Worcester, MA 01609

Technical Library
Applied Physics Laboratory
UNIVERSITY OF WASHINGTON
1013 N.E. 40th Street
Seattle, WA 98105

4 UNIVERSITY OF CALIFORNIA
Naval Architecture Department
Berkeley, CA 94720
Attn: Prof. W. Webster
Prof. J. Paulling
Prof. J. Wehausen
Library

3 CALIFORNIA INSTITUTE OF TECHNOLOGY
Pasadena, CA 91109
Attn: Dr. T.Y. Wu
Dr. A.J. Acosta
Library

Engineering Research Center
Reading Room
COLORADO STATE UNIVERSITY
Foothills Campus
Fort Collins, CO 80521

2 FLORIDA ATLANTIC UNIVERSITY
Ocean Engineering Department
Boca Raton, FL 33432
Attn: Technical Library
Dr. S. Dunne

Gordon McKay Library
HARVARD UNIVERSITY
Pierce Hall
Cambridge, MA 02138

Dept. of Ocean Engineering
Library
UNIVERSITY OF HAWAII
2565 The Mall
Honolulu, HI 96822

2 Institute of Hydraulic Research
THE UNIVERSITY OF IOWA
Iowa City, IA 52240
Attn: Library
Dr. L. Landweber

Fritz Engr Laboratory Library
Department of Civil Engineering
LEHIGH UNIVERSITY
Bethlehem, PA 18015

3 Department of Ocean Engineering
MASSACHUSETTS INSTITUTE OF TECHNOLOGY
Cambridge, MA 02139
Attn: Prof. P. Leehey
Prof. J. Newman
Prof. J. Kerwin

Engineering Technical Reports
Room 10-500
MASSACHUSETTS INSTITUTE OF TECHNOLOGY
Cambridge, MA 02139

2 St. Anthony Falls Hydraulic Lab
UNIVERSITY OF MINNESOTA
Mississippi River at 3rd Avenue S.E.
Minneapolis, MN 55414
Attn: Dr. Roger Arndt
Library

DISTRIBUTION LIST
(Contract N00014-77-C-0059)

2 Dept. of Naval Architecture and
Marine Engineering - North Campus
UNIVERSITY OF MICHIGAN
Ann Arbor, MI 48109
Attn: Library
Dr. T. Francis Ogilvie

2 Davidson Laboratory
STEVENS INSTITUTE OF TECHNOLOGY
711 Hudson Street
Hoboken, NJ 07030
Attn: Library
Dr. J. Breslin

Applied Research Laboratory Library
UNIVERSITY OF TEXAS
P.O. Box 8029
Austin, TX 78712

2 STANFORD UNIVERSITY
Stanford, CA 94305
Attn: Engineering Library
Dr. R. Street

Library
WEBB INSTITUTE OF NAVAL ARCHITECTURE
Crescent Beach Road
Glen Cove
Long Island, NY 11542

NATIONAL SCIENCE FOUNDATION
Engineering Division Library
1800 G Street N.W.
Washington, DC 20550

Dr. Douglas E. Humphreys, Code 794
NAVAL COASTAL SYSTEMS LABORATORY
Panama City, FL 32401

END

DATE
FILMED

1-81

DTIC